A fluid-dynamical model of the aorta with bifurcations

Olufsen, Mette; Ottesen, Johnny Tom

Publication date:
1995

Document Version
Publisher's PDF, also known as Version of record

Citation for published version (APA):
Olufsen, M., & Ottesen, J. T. (1995). *A fluid-dynamical model of the aorta with bifurcations*. Roskilde Universitet. Tekster fra IMFUFA No. 297 http://milne.ruc.dk/ImfufaTekster/

TEKST NR 297 1995

A fluid-dynamical model of the aorta with bifurcations

Mette Olufsen,
Johnny Ottesen

TEKSTER fra

IMFUFA ROSKILDE UNIVERSITETSCENTER
INSTITUT FOR STUDIET AF MATEMATIK OG FYSIK SAMT DERES
FUNKTIONER I UNDERVISNING, FORSKNING OG ANVENDELSER

Abstract

This report concerns a one-dimensional model of the blood flow in the major human arteries. This study is supposed to be used as a background for the design of a cardiovascular model used in the anaesthesia simulator developed by the SIMA group, consisting of members from the Bio-Math group at Roskilde University, the Simulator Section at Herlev University Hospital and Math-Tech ApS.

The first part of the report presents a basic model of the aorta regarded as an elastic, tapering tube. Flow and pressure of the blood are functions of time and (longitudinal) position in the tube and the blood is treated as an incompressible fluid. The model consists of a system of hyperbolic partial differential equations which are solved using two numerical techniques both based on finite difference schemes. Results from these are displayed and the methods are compared.

The second part presents a description of the outflow at the branches in the arterial network with special regard to the reflections from the iliac bifurcation, and results from this system is compared to the those of the basic model.

Preface

This report concerns an ongoing development of a one dimensional model of the blood flow in the major human arteries. The model is one of several to be included in an anaesthesia simulator. In a current implementation of the simulator a Windkessel model (zero dimensional) of the arteries is used. This includes a description of the capillary bed through a peripheral resistance.

In a next generation of the anaesthesia simulator the various submodels will be replaced by more detailed models based on physiological facts, which more adequately describe patients with pathological conditions. The simulator is used for training of anaesthesiologists and thus has to run in real time.

The one-dimensional model of the major arteries includes aorta, and several of the branches. In order to implement this submodel in the simulator it has to run faster than real time and it has to interface to the rest of the other submodels in the system. In a first implementation the outflow is described by a relation involving the peripheral resistance.

This report contains a background on how to make this one- dimensional model, and models for the aorta are described in detail, both regarding the system equations and possible numerical rutines needed for actually solving the equations.

This study is therefore regarded as a background research for the actual models that should be developed by the SIMA group consisting of The Simulator Section, Herlev University Hospital, The BioMath group, IMFUFA, Roskilde University and Math-Tech ApS. And we want to thank everybody in the SIMA group for their helpful comments throughout the work with this report.

Roskilde University, June, 1995

Mette Olufsen, and Johnny Ottesen

Contents

Chapter 1

A one-dimensional model of pulsatile flow in aorta

The work presented in this paper is motivated by the need for a physiologically based cardiovascular model in the anaesthesia simulator Sophus Jensen[5], Nielsen[10] and Olufsen[14], developed in the years 1991–93 in cooperation among Risø National Laboratory, Herlev University Hospital and Roskilde University. This work will provide a basis for a new cardiovascular model in the next generation of the anaesthesia simulator. This is being developed in the SIMA group which have participants from Herlev University Hospital (the Simulator Section), Roskilde University (the BioMath group), Math-Tech and S&W Medico Technics.

The topic of this paper is a treatment of the pressure and flow wave that emanates from the heart at each peak, and propagates toward the peripheral circulation through the arterial system. The interest is focussed on the flow in the large vessels, especially the aorta, where the Reynolds numbers are unusually high (of order 1000) even though the the flow in the human circulation in general remains laminar. Further, it is possible to treat the blood as a Newtonian fluid when dealing with the major arteries (when the diameter > 0.5 mm.). However, in the capillary flow this is not possible since the diameter of the vessels are small compared to the size of the red blood cells.

A number of people have worked on models of the pressure and flow wave generated as a result of an intermittent ejection of blood from the left ventricle. Most of the research in this field has taken place in the last few decades, Anliker[3] (1971), McDonald[9] (1974), Pedley[16] (1980), Stettler[24] (1981), Skalak[23] (1989), Lighthill[6] (1989), Reuderink[20] (1989), Zheng[29] (1993), and Paquerot[15] (1994). However, all were preceded by the work of W. Harvey from 1616, Noordergraaf[13], and Euler's early work from 1775, Skalak[23], published posthumously in 1862.

For a long time the development of the so called Windkessel theory was the primary focus. This describes a lumped system in which the arteries are represented by an elastic chamber that discharges through a fixed resistance representing the capillary bed, Skalak[23]. It seems that the representation of such a system often is made using an analogous electrical circuit model, Noordergraaf[12], Peskin[18], Sunagawa[26], Westerhof[27] and Westerhof[28]. The result of this modeling is a first-order approximation of pressure and flow at some specific points in the arteries. The advantage of this approach is the exclusive use of ordinary differential equations, that are easily simulated on a small computer. However, the lack of spatial information in the system makes it impossible to determine any continuous development of the flow, pressure and cross-sectional area. Instead, one must be satisfied with the values at particular key points represented in the model.

After the Windkessel theory was developed, an analysis using linearized wave propagation was initiated. Within this domain, two approaches have been carried out. The first approach dealt with a detailed analysis of the mode shapes and propagation velocities in which the blood and the vessel wall were treated as a three-dimensional continuum. The second approach described a one-dimensional analysis that to some extend included junctions and reflections, Skalak[23].

The cardiovascular model presented in the anaesthesia simulator Sophus is based on the Windkessel theory, Olufsen[14], and this approach does not fulfill the demands for the aims of the second generation simulator being developed by SIMA. Among other things it should be possible to investigate the exact regulation process of the fluid flow (which is dependent of the spatial development of the pressure wave), and the consequences of atherosclerosis at any given point.

In order to be able to deal with a continuous model not restricted to a linear system, we will make a one-dimensional model based on Navier Stokes equations. Eventually, it will cover an explicit description of the major bifurcations in the arterial tree. The small capillaries and the remainder of the bifurcations will be disregarded, since the model otherwise will be too comprehensive.

So far this paper covers a model of the aorta, primarily based on the work by Anliker in [2] and [3], and Stettler[25]. The aorta is modeled as an elastic tapering tube. The blood is handled as an incompressible inviscous fluid, and the complete description of the system contains a momentum equation (Euler's equation expanded with a heterogeneous friction term proportional to the Poiseuille friction), a continuity equation, and a state equation (an elasticity function, that relates the pressure to the cross-sectional area). These equations are solved numerically using two different finite difference methods. One based on the method of characteristics, Ralston[7] and the other is Lax Wendroff's two-step method (Richtmayer's version), Peskin[17]. The results from these two methods are compared, and the convergence is investigated. Finally, a model of the branching system is considered and two methods are proposed and evaluated.

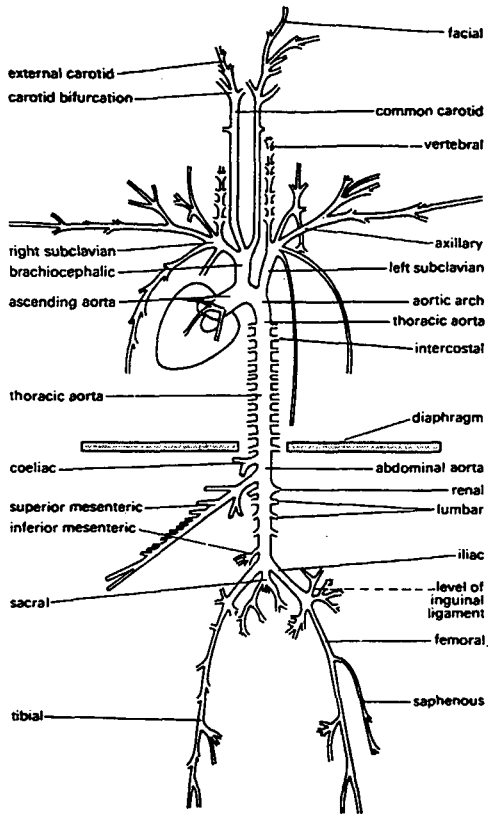

Figure 1.1: Major branches of the canine arterial tree, from McDonald[9]. The vessel modeled in this section contains the aorta (starting just below the aortic arch), and the abdominal aorta ending at the iliac bifurcation.

1.1 The aorta model

In this section we will concentrate on setting up the equations governing the flow in aorta. These are a momentum equation, a continuity equation, and a state equation. Figure 1.1 gives an intuitive understanding of the human arterial system. However, it shows the quite similar arterial system of a canine. The model presented in this section regards the aorta starting immediately after the aortic arch and ending at the iliac bifurcation.

1.1.1 The system equations

The momentum equation consists of Euler's equation added a friction term:

$$\frac{\partial u}{\partial t} + u\frac{\partial u}{\partial x} + \frac{1}{\rho}\frac{\partial p}{\partial x} = \frac{F}{\rho} \tag{1.1}$$

where $u(x,t)$ is the mean velocity over the cross-sectional area, $p(x,t)$ is the mean pressure, ρ is the density (constant), and $\frac{F}{\rho}$ is the friction, that arises due to our

assumption of Poiseuille flow. It is given by

$$-8k\pi\frac{\mu u}{\rho A}$$

where μ is the viscosity, A is the cross-sectional area of the tube, and k is a proportionality factor.

The continuity equation is

$$\frac{\partial A}{\partial t}+\frac{\partial Au}{\partial x} = 0 \tag{1.2}$$

The momentum equation can be represented as a function of the flow $Q = Au$, by multiplying (1.1) with A, (1.2) with u, and adding the two equations. Hence

$$\frac{\partial Q}{\partial t}+\frac{\partial}{\partial x}\frac{Q^2}{A}+\frac{A}{\rho}\frac{\partial p}{\partial x} = \tilde{F} \tag{1.3}$$

where $\tilde{F} = \frac{FA}{\rho} = -8k\pi\frac{\mu u}{\rho}$. In the following we will reuse the symbol F for $\tilde{F}$. Expansion of the term $\frac{\partial}{\partial x}\frac{Q^2}{A}$ in terms of Q and A results in the following quasi-linear partial differential equation:

$$\frac{\partial Q}{\partial t}+\frac{2Q}{A}\frac{\partial Q}{\partial x}-\frac{Q^2}{A^2}\frac{\partial A}{\partial x}+\frac{A}{\rho}\frac{\partial p}{\partial x} = F \tag{1.4}$$

The state equation is according to Mazumdar[8] page 130 given by

$$p = \frac{EW}{r}\left(1-\sqrt{\frac{A_0}{A}}\right)+p_0 \tag{1.5}$$

where p_0 is the pressure of the surroundings, r is the radius of aorta, $A_0 = \pi r^2$ is the cross-sectional area at the pressure p_0, W is the thickness of the wall and E is Young's modulus. However, if one compares a plot of p versus A with data measured (from Anliker[2] page 30 or Noordergraaf[11] page 116) this equation does not have the right appearance. In fact the relation should form a hysteresis cycle between the systolic and the diastolic pressure, in figure 1.2 the relation from Anliker[2] is showed as opposed to our relationship. Therefore one should consider some other approach that takes this property into account.

Since the tube is tapering, the radius r is a function of x. It is given by Anliker[3], page 225

$$r = ae^{-bx}$$

where a and b are determined according to the specified radius at the top and bottom of the aorta.

Using (1.5) the critical excess pressure can be defined as

$$p_c = \lim_{A \to \infty} p = \lim_{A \to \infty} \frac{EW}{r} \left(1 - \sqrt{\frac{A_0}{A}}\right) = \frac{EW}{r} \tag{1.6}$$

Hence, the relative excess pressure can be expressed as

$$p_E = \frac{p - p_0}{p_c} = 1 - \sqrt{\frac{A_0}{A}} \tag{1.7}$$

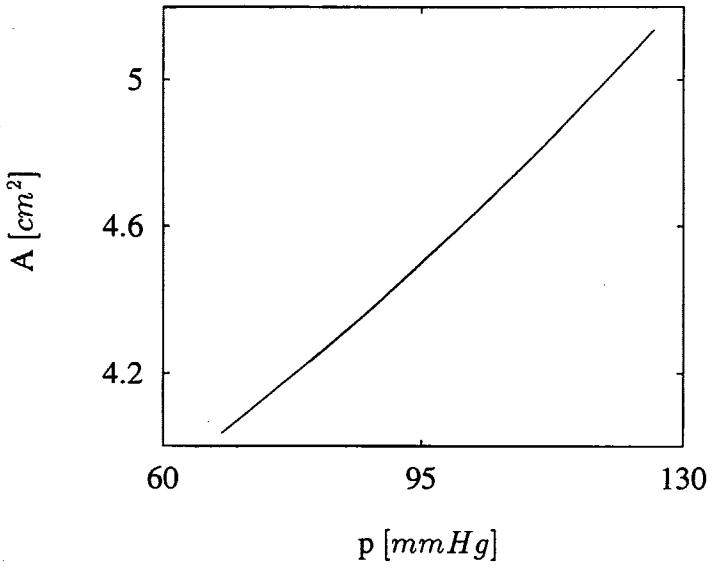

Figure A

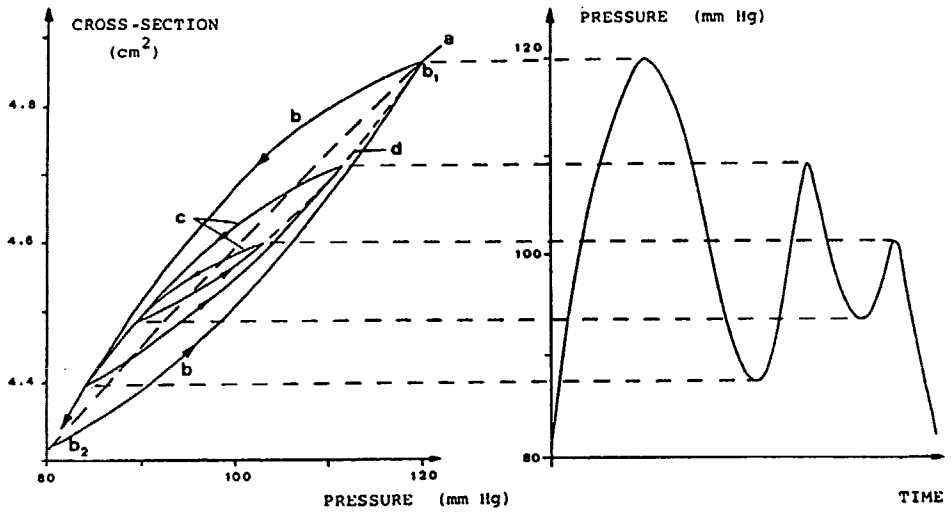

Figure B

Figure 1.2: The viscoelastic behavior of the wall. The plots show the cross-sectional area as a function of the pressure in a non-tapered tube. A shows the relationship used in our work (using the same parameters as in figure 3.1 but without the taper) and B (from Anliker[2]) shows the hysteresis cycle between the systolic and the diastolic pressures. a: the original elastic curve, b: the master hysteresis cycle between systolic (b_1) and diastolic (b_2) pressures. c: higher order cycles that emanates from the reflections of the pressure wave. d: path leading back to the master cycle. The depicted situation results from the hypothetic pressure pulse shown.

The derivative of p with respect to x is

$$\begin{aligned}\frac{\partial p}{\partial x} &= \frac{\partial p}{\partial A}\frac{\partial A}{\partial x} + \frac{\partial p}{\partial A_0}\frac{dA_0}{dx} + \frac{\partial p}{\partial p_c}\frac{dp_c}{dx} \\ &= \frac{p_c}{2}\sqrt{\frac{A_0}{A^3}}\frac{\partial A}{\partial x} - \frac{p_c}{r}\frac{dr}{dx} + \left(\frac{1}{r} - \sqrt{\frac{\pi}{A}}\right)\frac{dEW}{dx}\end{aligned} \tag{1.8}$$

We are now ready to write the system of equations that should be solved. This consists of the continuity equation (1.2) and the momentum equation (1.4), and using (1.8) we get.

$$\frac{\partial}{\partial t}\begin{pmatrix} A \\ Q \end{pmatrix} + \begin{pmatrix} 0 & 1 \\ \frac{p_c}{2\rho}\sqrt{\frac{A_0}{A}} - \frac{Q^2}{A^2} & \frac{2Q}{A} \end{pmatrix}\frac{\partial}{\partial x}\begin{pmatrix} A \\ Q \end{pmatrix} = \begin{pmatrix} 0 \\ F + \frac{Ap_c}{\rho r}\frac{dr}{dx} - \frac{1}{\rho}\left(\frac{A}{r} - \sqrt{\pi A}\right)\frac{dEW}{dx} \end{pmatrix} \tag{1.9}$$

In order to put the equations (1.2) and (1.3) into conservation form, which is needed in order to apply Lax Wendroff's two-step method, we introduce the quantity B chosen to fulfill

$$\frac{\partial B}{\partial p} = \frac{A(p(t,x), p_c(x), A_0(x))}{\rho}$$

Then

$$B(p, p_c, A_0) = \frac{1}{\rho}\int A\, dp$$

The derivative with respect to x is

$$\frac{\partial B}{\partial x} = \frac{\partial B}{\partial p}\frac{\partial p}{\partial x} + \frac{\partial B}{\partial A_0}\frac{dA_0}{dx} + \frac{\partial B}{\partial p_c}\frac{dp_c}{dx} \tag{1.10}$$

The momentum equation (1.3) can be rewritten using (1.10), since the term $\frac{A}{\rho}\frac{\partial p}{\partial x}$ can be expressed using $\frac{\partial B}{\partial p}\frac{\partial p}{\partial x}$. Because the last two terms in (1.10) do not contain any partial derivatives of p (and hence A) and Q, they can be evaluated directly and may therefore be added to both sides of (1.3). Consequently,

$$\frac{\partial Q}{\partial t} + \frac{\partial}{\partial x}\left(\frac{Q^2}{A} + B\right) = F + \frac{\partial B}{\partial A_0}\frac{dA_0}{dx} + \frac{\partial B}{\partial p_c}\frac{dp_c}{dx}$$

Using the definitions (1.5) and (1.6) of p and p_c, we evaluate the function B as

$$B = \frac{A_0}{\rho}\int \frac{1}{\left(1 - \frac{p-p_0}{p_c}\right)^2} dp = \frac{A_0 p_c}{\rho\left(1 - \frac{p-p_0}{p_c}\right)} = \frac{A_0 p_c}{\rho\left(1 - p_E\right)}$$

Finally the terms $\frac{\partial B}{\partial A_0}\frac{dA_0}{dx}$ and $\frac{\partial B}{\partial p_c}\frac{dp_c}{dx}$ must be evaluated:

$$\frac{\partial B}{\partial A_0}\frac{dA_0}{dx} = \frac{p_c}{\rho(1-p_E)}2\pi r\frac{dr}{dx}$$

and

$$\begin{aligned}\frac{\partial B}{\partial p_c}\frac{dp_c}{dx} &= \frac{\rho\left(1-\frac{p-p_0}{p_c}\right)A_0 - A_0 p_c \rho\frac{p-p_0}{p_c^2}}{\rho^2\left(1-\frac{p-p_0}{p_c}\right)^2}\left(\frac{1}{r}\frac{dEW}{dx} - \frac{EW}{r^2}\frac{dr}{dx}\right)\\ &= \frac{A(1-2p_E)}{r\rho}\left(\frac{dEW}{dx} - p_c\frac{dr}{dx}\right)\end{aligned}$$

The system of equations in conservation form can thus be written as

$$\frac{\partial}{\partial t}\begin{pmatrix} A \\ Q \end{pmatrix} + \frac{\partial}{\partial x}\begin{pmatrix} Q \\ \frac{Q^2}{A} + \frac{A_0 p_c}{\rho(1-p_E)} \end{pmatrix} = \begin{pmatrix} 0 \\ F + \frac{\partial B}{\partial A_0}\frac{dA_0}{dx} + \frac{\partial B}{\partial p_c}\frac{dp_c}{dx} \end{pmatrix} \tag{1.11}$$

where the term $\frac{\partial B}{\partial A_0}\frac{dA_0}{dx} + \frac{\partial B}{\partial p_c}\frac{dp_c}{dx}$ is given by

$$\begin{aligned}&\left(\frac{2\pi r}{1-p_E} - \frac{A(1-2p_E)}{r}\right)\frac{p_c}{\rho}\frac{dr}{dx} + \frac{A(1-2p_E)}{r\rho}\frac{dEW}{dx} =\\ &\frac{Ap_c}{r\rho}\frac{dr}{dx} + \frac{2\sqrt{AA_0}-A}{r\rho}\frac{dEW}{dx} =\\ &\frac{Ap_c}{r\rho}\frac{dr}{dx} + \frac{1}{\rho}\left(2\sqrt{\pi A} - \frac{A}{r}\right)\frac{dEW}{dx}\end{aligned}$$

The numerical treatment of these equations will, as mentioned, be carried out in two ways, both based on finite difference methods. The first method considered is Richtmayer's version of Lax Wendroff's two-step method, Peskin[17], and the second is based on the method of characteristics, Ralston[7].

In both cases the equations are treated in non-dimensional form. In order to do so, we apply the following characteristic parameters:

- $L = 76\ [cm]$, the characteristic length of aorta.
- $q = 70\ [cm^3 s^{-1}]$, the characteristic flow through aorta (taken as the desired cardiac output).
- $g = 981\ [cms^{-2}]$, the gravitational constant.
- $\rho = 1.06\ [gcm^{-3}]$, the density of the blood.

The latter two parameters are used in order to determine a characteristic pressure $\rho g L$ $[gs^{-2}cm^{-1}]$ which equals $\frac{760}{101.3 \cdot 10^4}$ $[mmHg]$.

The non-dimensional form of (1.9) is given by

$$\frac{\partial}{\partial t}\begin{pmatrix} A \\ Q \end{pmatrix} + \begin{pmatrix} 0 & 1 \\ \frac{p_c}{2\mathcal{F}^2}\sqrt{\frac{A_0}{A}} - \frac{Q^2}{A^2} & \frac{2Q}{A} \end{pmatrix} \frac{\partial}{\partial x}\begin{pmatrix} A \\ Q \end{pmatrix} = \begin{pmatrix} 0 \\ F + \frac{Ap_c}{\mathcal{F}^2 r}\frac{dr}{dx} + \frac{1}{\mathcal{F}^2}\left(\sqrt{\pi A} - \frac{A}{r}\right)\frac{dEW}{dx} \end{pmatrix} \tag{1.12}$$

where $\mathcal{F} = \sqrt{\frac{q^2}{gL^5}}$. The non-dimensional friction term is

$$F = -8k\pi \frac{1}{\mathcal{R}}\frac{Q}{A} \tag{1.13}$$

where $\mathcal{R} = \frac{\rho q}{\mu L}$.

The non-dimensional form of the conservative system (1.11) is given by

$$\frac{\partial}{\partial t}\begin{pmatrix} A \\ Q \end{pmatrix} + \frac{\partial}{\partial x}\begin{pmatrix} Q \\ \frac{Q^2}{A} + \frac{A_0 p_c}{\mathcal{F}^2(1-p_E)} \end{pmatrix} = \begin{pmatrix} 0 \\ F + \frac{Ap_c}{r\mathcal{F}^2}\frac{dr}{dx} + \frac{1}{\mathcal{F}^2}\left(2\sqrt{\pi A} - \frac{A}{r}\right)\frac{dEW}{dx} \end{pmatrix} \tag{1.14}$$

where F is as given in (1.13).

The Reynolds number characterizing the flow is given by:

$$\mathcal{R} = \frac{\rho q}{\mu r} \approx 1514$$

where r is a characteristic radius of aorta. It is taken to be 1 cm. Since we are using a constant density and viscosity this radius only varies little due to the tapering of the tube.

1.2 Lax Wendroff's two-step method

This is a second-order method[1] dealing with the equations given in conservation form (1.14). In addition, the pressure terms in the system of equations must be rewritten in terms of the cross-sectional area A. Consequently, the equations will be

$$\frac{\partial}{\partial t}\begin{pmatrix} A \\ Q \end{pmatrix} + \frac{\partial}{\partial x}\begin{pmatrix} Q \\ \frac{Q^2}{A} + \frac{p_c\sqrt{A_0 A}}{\mathcal{F}^2} \end{pmatrix} = \begin{pmatrix} 0 \\ F + \frac{Ap_c}{r\mathcal{F}^2}\frac{dr}{dx} + \frac{1}{\mathcal{F}^2}\left(2\sqrt{\pi A} - \frac{A}{r}\right)\frac{dEW}{dx} \end{pmatrix} \tag{1.15}$$

[1] A more detailed analysis of the stability of this method should be conducted.

In order to write the finite difference equations we need the following definitions.

Let the dependent variables be represented in the vector $\mathbf{U}$.

$$\mathbf{U} = (A, Q)$$

The system flux is

$$\mathbf{R} = (R_1, R_2) = \left(Q, \frac{Q^2}{A} + \frac{p_c\sqrt{A_0 A}}{\mathcal{F}^2}\right) \tag{1.16}$$

and the right hand side of the system is represented by the vector

$$\mathbf{S} = (S_1, S_2) = \left(0, F + \frac{Ap_c}{r\mathcal{F}^2}\frac{dr}{dx} + \frac{1}{\mathcal{F}^2}\left(2\sqrt{\pi A} - \frac{A}{r}\right)\frac{dEW}{dx}\right) \tag{1.17}$$

The system of equations (1.15) may then be written as

$$\frac{\partial}{\partial t}\mathbf{U} + \frac{\partial}{\partial x}\mathbf{R} = \mathbf{S} \tag{1.18}$$

The time step is defined by $k = \Delta t$ and the space step by $h = \Delta x$. Let $\mathbf{U}_j^n = \mathbf{U}(jh, nk)$ and similarly for $\mathbf{R}$ and $\mathbf{S}$. Using a uniform grid, one can derive a four point formula, using two intermediate points at $(\mathbf{U})_{j+\frac{1}{2}}^{n+\frac{1}{2}}$:

$$\mathbf{U}_{j+\frac{1}{2}}^{n+\frac{1}{2}} = \frac{1}{2}\left(\mathbf{U}_{j+1}^n + \mathbf{U}_j^n\right) + \frac{k}{2}\left(-\frac{\mathbf{R}_{j+1}^n - \mathbf{R}_j^n}{h} + \frac{\mathbf{S}_{j+1}^n + \mathbf{S}_j{}^n}{2}\right) \tag{1.19}$$

from $\mathbf{U}_{j+\frac{1}{2}}^{n+\frac{1}{2}}$ it is possible to derive $\mathbf{R}_{j+\frac{1}{2}}^{n+\frac{1}{2}}$ and $\mathbf{S}_{j+\frac{1}{2}}^{n+\frac{1}{2}}$ according to the definitions in (1.16) and (1.17). Similarly, $\mathbf{R}_{j-\frac{1}{2}}^{n+\frac{1}{2}}$ and $\mathbf{S}_{j-\frac{1}{2}}^{n+\frac{1}{2}}$ can be derived from $\mathbf{U}_{j-\frac{1}{2}}^{n+\frac{1}{2}}$.

It is now possible to determine $\mathbf{U}_j^{n+1}$ by:

$$\mathbf{U}_j^{n+1} = \mathbf{U}_j^n - \frac{k}{h}\left(\mathbf{R}_{j+\frac{1}{2}}^{n+\frac{1}{2}} - \mathbf{R}_{j-\frac{1}{2}}^{n+\frac{1}{2}}\right) + \frac{k}{2}\left(\mathbf{S}_{j+\frac{1}{2}}^{n+\frac{1}{2}} + \mathbf{S}_{j-\frac{1}{2}}^{n+\frac{1}{2}}\right) \tag{1.20}$$

The general grid used is displayed in figure (1.2).

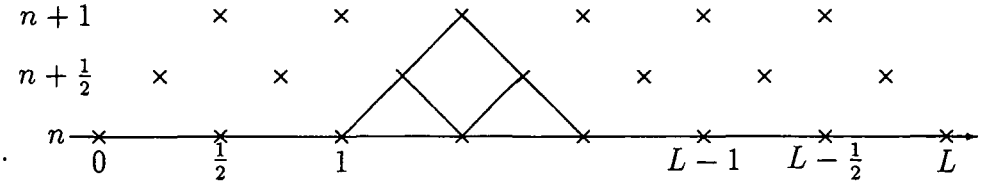

Figure 1.3: In order to determine the values of Q and A at $n+1$, the intermediate values defined in (1.19) must be determined first.

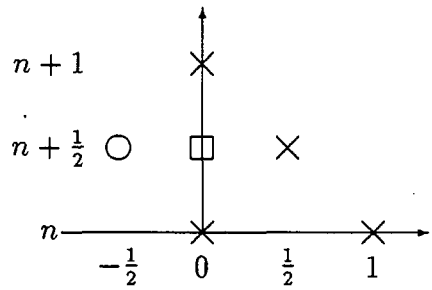

Figure 1.4: Left boundary: All variables are known at the points marked with a cross. In order to determine the value of A_0^{n+1}, we apply the boundary condition for $Q_0^{n+\frac{1}{2}}$ at the point marked with a square, and from this it is possible to determine an approximate value at the ghost point marked with a circle. The latter is done by taking the average of the point marked by a circle and the point $(\frac{1}{2}, n+\frac{1}{2})$. The value of Q_0^{n+1} can then be found using this construction and the boundary condition.

1.3 The Boundary Conditions

1.3.1 The left boundary

In order to ensure a reasonable cardiac ejection rate at the proximal end of the aorta, this boundary condition is given by

$$Q(0,t) = Q_0(t) = (\alpha \sin(\beta t))_{x=0} \tag{1.21}$$

where the constants α and β can be determined from the knowledge of the cardiac output and the period of one heart beat.

The corresponding non-dimensional boundary condition is

$$Q_0(t) = \left(\frac{\alpha}{q} \sin\left(\beta \frac{L^3}{q} t\right)\right)_{x=0}$$

where L is a characteristic length of the tube, and q is a characteristic flow.

In order to determine A at the left boundary, we need a value of Q at the ghost point marked by a circle on figure 1.4. This can be done using the approximation

$$\begin{aligned} Q_0^{n+\frac{1}{2}} &= \frac{1}{2}\left(Q_{-\frac{1}{2}}^{n+\frac{1}{2}} + Q_{\frac{1}{2}}^{n+\frac{1}{2}}\right) \quad \Leftrightarrow \\ Q_{-\frac{1}{2}}^{n+\frac{1}{2}} &= 2Q_0^{n+\frac{1}{2}} - Q_{\frac{1}{2}}^{n+\frac{1}{2}} \end{aligned} \tag{1.22}$$

We are now able to determine A using Lax Wendroff's scheme from (1.20).

$$A_0^{n+1} = A_0^n - \frac{k}{h}\left((R_1)_{\frac{1}{2}}^{n+\frac{1}{2}} - (R_1)_{-\frac{1}{2}}^{n+\frac{1}{2}}\right) + \frac{k}{2}\left((S_1)_{\frac{1}{2}}^{n+\frac{1}{2}} + (S_1)_{-\frac{1}{2}}^{n+\frac{1}{2}}\right)$$

In this scheme the only unknowns are $(R_1)_{-\frac{1}{2}}^{n+\frac{1}{2}}$ and $(S_1)_{-\frac{1}{2}}^{n+\frac{1}{2}}$, and from (1.16) and (1.17), they are given by

$$(R_1)_{-\frac{1}{2}}^{n+\frac{1}{2}} = Q_{-\frac{1}{2}}^{n+\frac{1}{2}} \quad \text{and} \quad (S_1)_{-\frac{1}{2}}^{n+\frac{1}{2}} = 0$$

1.3.2 The right boundary

The peripheral boundary condition is, chosen according to the approach suggested by Anliker[3], namely

$$Q(x_L, t) = Q_L(t) = \left(\frac{p - p_e}{R_L}\right)_{x=x_L} = \left(\frac{p_c\left(1 - \sqrt{\frac{A_0}{A}}\right) + p_0 - p_e}{R_L}\right)_{x=x_L} \tag{1.23}$$

where p_e is the end-capillary pressure, and R_L is the outflow resistance. The dimension less boundary condition is analogous, but contains the corresponding non-dimensional quantities.

The problem with this approach is the assumption that the peripheral resistance is constant. This is not strictly physiologically true, but it is difficult to determine R_L as an explicit function of time. In fact, Peskin argues that the pressure is approximately proportional to the flow far away from the heart, but it is also true that there is a lack of such condition near the heart, Peskin[17]. Therefore, and since the model is very sensitive to this choice, it should be investigated further. However, in this report we have chosen to use the simple boundary condition.

Treating the right boundary condition is a little more tricky, since $Q(x_L, t)$ is not known explicitly, but only as a function of the unknown p (and hence A).

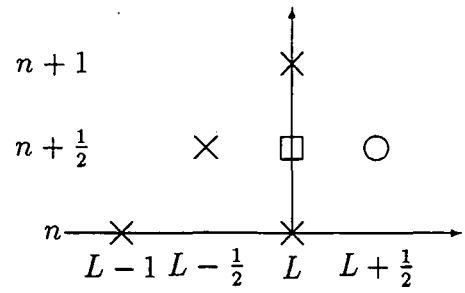

Figure 1.5: Right boundary: All variables are known at the points marked with a cross. In order to have enough equations to determine the values of Q and A at $(L, n+1)$, we need to add a ghost point, marked with a circle, and use the boundary condition at the point marked with a square. Similarly to the left boundary we determine the value at the point marked with a circle by averaging the square point over this and the point $(L-\frac{1}{2}, n+\frac{1}{2})$.

From the numerical scheme in (1.20) we have got the following relations:

$$\begin{aligned} A_L^{n+1} &= A_L^n - \frac{k}{h}\left((R_1)_{L+\frac{1}{2}}^{n+\frac{1}{2}} - (R_1)_{L-\frac{1}{2}}^{n+\frac{1}{2}}\right) + \\ &\quad \frac{k}{2}\left((S_1)_{L+\frac{1}{2}}^{n+\frac{1}{2}} + (S_1)_{L-\frac{1}{2}}^{n+\frac{1}{2}}\right) \\ &= A_L^n - \frac{k}{h}\left((R_1)_{L+\frac{1}{2}}^{n+\frac{1}{2}} - (R_1)_{L-\frac{1}{2}}^{n+\frac{1}{2}}\right) \end{aligned} \tag{1.24}$$

since $S_1 = 0$, and

$$\begin{aligned} Q_L^{n+1} &= Q_L^n - \frac{k}{h}\left((R_2)_{L+\frac{1}{2}}^{n+\frac{1}{2}} - (R_2)_{L-\frac{1}{2}}^{n+\frac{1}{2}}\right) + \\ &\quad \frac{k}{2}\left((S_2)_{L+\frac{1}{2}}^{n+\frac{1}{2}} + (S_2)_{L-\frac{1}{2}}^{n+\frac{1}{2}}\right) \end{aligned} \tag{1.25}$$

The unknowns in these equations are Q_L^{n+1}, A_L^{n+1}, $(\mathbf{R})_{L+\frac{1}{2}}^{n+\frac{1}{2}}$ and $(S_2)_{L+\frac{1}{2}}^{n+\frac{1}{2}}$. However, $(\mathbf{R})_{L+\frac{1}{2}}^{n+\frac{1}{2}}$ and $(S_2)_{L+\frac{1}{2}}^{n+\frac{1}{2}}$ are both functions of $Q_{L+\frac{1}{2}}^{n+\frac{1}{2}}$ and $A_{L+\frac{1}{2}}^{n+\frac{1}{2}}$. In order to determine these values we need to establish a ghost point (marked with a circle on figure 1.5), and similar to the left boundary we make the relations:

$$Q_L^{n+\frac{1}{2}} = \frac{Q_{L-\frac{1}{2}}^{n+\frac{1}{2}} + Q_{L+\frac{1}{2}}^{n+\frac{1}{2}}}{2} \tag{1.26}$$

$$A_L^{n+\frac{1}{2}} = \frac{A_{L-\frac{1}{2}}^{n+\frac{1}{2}} + A_{L+\frac{1}{2}}^{n+\frac{1}{2}}}{2} \tag{1.27}$$

However, these equations add two more unknowns, namely $Q_L^{n+\frac{1}{2}}$ and $A_L^{n+\frac{1}{2}}$ to the system. Therefore we need two more equations. These can be found using the boundary

condition at the time levels $n+\frac{1}{2}$ and $n+1$.

$$Q_L^{n+\frac{1}{2}} = \frac{(p_c)_L\left(1-\sqrt{\frac{(A_0)_L}{A_L^{n+\frac{1}{2}}}}\right)-p_e+p_0}{R_L} \tag{1.28}$$

$$Q_L^{n+1} = \frac{(p_c)_L\left(1-\sqrt{\frac{(A_0)_L}{A_L^{n+1}}}\right)-p_e+p_0}{R_L} \tag{1.29}$$

The subscripts and superscripts are only mentioned if the respective variables depend on the corresponding parameter.

We will now solve the six equations (1.24-1.29) having the six unknowns Q_L^{n+1}, A_L^{n+1}, $Q_L^{n+\frac{1}{2}}$, $A_L^{n+\frac{1}{2}}$, $Q_{L+\frac{1}{2}}^{n+\frac{1}{2}}$, and $A_{L+\frac{1}{2}}^{n+\frac{1}{2}}$.

In order to reduce the number of equations we make a simplification, substituting equations (1.26) and (1.27) into (1.28). Hence, equation (1.28) can be rewritten as:

$$\frac{Q_{L-\frac{1}{2}}^{n+\frac{1}{2}}+Q_{L+\frac{1}{2}}^{n+\frac{1}{2}}}{2} = \frac{(p_c)_L\left(1-\sqrt{\frac{2(A_0)_L}{A_{L-\frac{1}{2}}^{n+\frac{1}{2}}+A_{L+\frac{1}{2}}^{n+\frac{1}{2}}}}\right)+p_0-p_e}{R_L} \tag{1.30}$$

The four equations to be solved are thus (1.24), (1.25), (1.29), and (1.30), and the unknowns are $Q_{L+\frac{1}{2}}^{n+\frac{1}{2}}$, $A_{L+\frac{1}{2}}^{n+\frac{1}{2}}$, Q_L^{n+1}, and A_L^{n+1}.

Let

$$x_1 = Q_{L+\frac{1}{2}}^{n+\frac{1}{2}} \quad x_2 = A_{L+\frac{1}{2}}^{n+\frac{1}{2}}$$
$$x_3 = Q_L^{n+1} \quad x_4 = A_L^{n+1}$$

Equation 1: Consider the residue defined as f_1 derived from (1.30).

$$f_1 = \frac{(p_c)_L\left(1-\sqrt{\frac{2(A_0)_L}{A_{L-\frac{1}{2}}^{n+\frac{1}{2}}+x_2}}\right)+p_0-p_e}{R_L} - \frac{Q_{L-\frac{1}{2}}^{n+\frac{1}{2}}+x_1}{2} \tag{1.31}$$

Let

$$g_1 = \frac{(p_c)_L+p_0-p_e}{R_L} - \frac{Q_{L-\frac{1}{2}}^{n+\frac{1}{2}}}{2}$$

$$g_2 = \frac{(p_c)_L\sqrt{2\,(A_0)_L}}{R_L}$$

f_1 can then be rewritten as:

$$f_1 = g_1 - \frac{g_2}{\sqrt{A_{L-\frac{1}{2}}^{n+\frac{1}{2}} + x_2}} - \frac{x_1}{2} \tag{1.32}$$

Equation 2: Similarly, the residue f_2 obtained from (1.29) is

$$f_2 = \frac{(p_c)_L \left(1 - \sqrt{\frac{(A_0)_L}{x_4}}\right) + p_0 - p_e}{R_L} - x_3 \tag{1.33}$$

Let

$$\begin{aligned} g_3 &= \frac{(p_c)_L + p_0 - p_e}{R_L} \\ g_4 &= \frac{(p_c)_L \sqrt{(A_0)_L}}{R_L} \end{aligned}$$

f_2 can therefore be rewritten as:

$$f_2 = g_3 - \frac{g_4}{\sqrt{x_4}} - x_3$$

Equation 3: The residue derived from (1.24) is

$$f_3 = A_L^n - \frac{k}{h}\left(x_1 - (R_1)_{L-\frac{1}{2}}^{n+\frac{1}{2}}\right) - x_4 \tag{1.34}$$

Let

$$\begin{aligned} \theta &= \frac{k}{h} \\ \gamma &= \frac{k}{2} \\ g_5 &= A_L^n + \theta\,(R_1)_{L-\frac{1}{2}}^{n+\frac{1}{2}} \end{aligned}$$

f_3 can thus be rewritten as:

$$f_3 = g_5 - \theta x_1 - x_4$$

Equation 4: Finally, the residue obtained from (1.25) is

$$f_4 = -x_3 + Q_L^n - \frac{k}{h}\left(\left(\frac{x_1^2}{x_2} + \frac{p_c\sqrt{A_0 x_2}}{\mathcal{F}^2}\right)_{L+\frac{1}{2}}^{n+\frac{1}{2}} - (R_2)_{L-\frac{1}{2}}^{n+\frac{1}{2}}\right) + \frac{k}{2}\left(\left(F + \frac{x_2 p_c}{r\mathcal{F}^2}\frac{dr}{dx} + \frac{2\sqrt{A_0 x_2} - x_2}{r\mathcal{F}^2}\frac{dEW}{dx}\right)_{L+\frac{1}{2}}^{n+\frac{1}{2}} + (S_2)_{L-\frac{1}{2}}^{n+\frac{1}{2}}\right) \quad (1.35)$$

From (1.13) we have

$$F = -8k\pi\frac{1}{\mathcal{R}}\frac{x_1}{x_2}$$

Let

$$k_1 = \left(\frac{p_c\sqrt{A_0}}{\mathcal{F}^2}\right)_{L+\frac{1}{2}}$$

$$k_2 = -8k\pi\frac{1}{\mathcal{R}}$$

$$k_3 = \left(\frac{2\sqrt{A_0}}{r\mathcal{F}^2}\frac{dEW}{dx}\right)_{L+\frac{1}{2}}$$

$$k_4 = \left(\frac{p_c}{r\mathcal{F}^2}\frac{dr}{dx} - \frac{1}{r\mathcal{F}^2}\frac{dEW}{dx}\right)_{L+\frac{1}{2}}$$

In the computations done so far EW is constant[2], so k_3 and the last term of k_4 vanishes. When all the constants k_i are evaluated at the point $(L+\frac{1}{2}, n+\frac{1}{2})$ then f_4 can be rewritten as:

$$f_4 = -x_3 + Q_L^n - \theta\left(\frac{x_1^2}{x_2} + k_1\sqrt{x_2} - (R_2)_{L-\frac{1}{2}}^{n+\frac{1}{2}}\right) + \gamma\left(k_2\frac{x_1}{x_2} + k_3\sqrt{x_2} + k_4 x_2 + (S_2)_{L-\frac{1}{2}}^{n+\frac{1}{2}}\right)$$

If

$$g_6 = Q_L^n + \theta\,(R_2)_{L-\frac{1}{2}}^{n+\frac{1}{2}} + \gamma\,(S_2)_{L-\frac{1}{2}}^{n+\frac{1}{2}}$$

then the final form of f_4 is given by:

$$f_4 = -x_3 + g_6 - \theta\left(\frac{x_1^2}{x_2} + k_1\sqrt{x_2}\right) + \gamma\left(k_2\frac{x_1}{x_2} + k_3\sqrt{x_2} + k_4 x_2\right)$$

[2] An investigation of this assumption should be conducted.

It is now possible to find $x_1 - x_4$ using Newton's method (See either [19] page 379ff. or [4] page 261ff.). This method is defined by the following first-order accurate scheme:

$$\mathbf{x}_{i+1} = \mathbf{x}_i - (D\mathbf{f}(\mathbf{x}_i))^{-1}\,\mathbf{f}(\mathbf{x}_i), \quad i = 0, 1, 2, 3, \ldots \tag{1.36}$$

where the indices i refer to the number of iterations, and $\mathbf{x}$ is the vector (x_1, x_2, x_3, x_4). However, this method is only good if the Jacobian of $D\mathbf{f}(\mathbf{x}_0)$ is nonsingular, and if it is possible to come up with a good initial guess for $\mathbf{x}_0$. In this case the initial guess can be chosen as

$$\begin{aligned} (x_1)_0 &= Q_L^n, \quad (x_2)_0 = A_L^n \\ (x_3)_0 &= Q_{L-\frac{1}{2}}^{n+\frac{1}{2}}, \quad (x_4)_0 = A_{L-\frac{1}{2}}^{n+\frac{1}{2}} \end{aligned}$$

since we assume that $\mathbf{x}$ does not change too rapidly during a half time step.

The Jacobian is given by:

$$D\mathbf{f} = \begin{pmatrix} \frac{\partial f_1}{\partial x_1} & \frac{\partial f_1}{\partial x_2} & \frac{\partial f_1}{\partial x_3} & \frac{\partial f_1}{\partial x_4} \\ \frac{\partial f_2}{\partial x_1} & \cdot & \cdot & \cdot \\ \frac{\partial f_3}{\partial x_1} & \cdot & \cdot & \cdot \\ \frac{\partial f_4}{\partial x_1} & \cdot & \cdot & \frac{\partial f_4}{\partial x_4} \end{pmatrix}$$

with the values:

$$D\mathbf{f} = \begin{pmatrix} -\frac{1}{2} & \frac{g_2}{2\left(A_{L-\frac{1}{2}}^{n+\frac{1}{2}} + x_2\right)^{3/2}} & 0 & 0 \\ 0 & 0 & -1 & \frac{g_4}{2x_4^{3/2}} \\ -\theta & 0 & 0 & -1 \\ -2\theta\frac{x_1}{x_2} + \gamma\frac{k_2}{x_2} & \theta\left(\left(\frac{x_1}{x_2}\right)^2 - \frac{1}{2}\frac{k_1}{\sqrt{x_2}}\right) + \gamma\left(-k_2\frac{x_1}{x_2^2} + \frac{1}{2}\frac{k_3}{\sqrt{x_2}} + k_4\right) & -1 & 0 \end{pmatrix}$$

1.4 The method of characteristics

In order to apply the method of characteristics to the equations, we use the form given in (1.12). Let $(t, x(t))$ describe the desired curve in the (t, x) plane.

If we let $a = \frac{dx}{dt}$ we have the following identity:

$$\frac{d}{dt}\begin{pmatrix} A \\ Q \end{pmatrix} = \frac{\partial}{\partial t}\begin{pmatrix} A \\ Q \end{pmatrix} + a\frac{\partial}{\partial x}\begin{pmatrix} A \\ Q \end{pmatrix} \tag{1.37}$$

The solution to the system in (1.12) along the chosen curve resulting in the identity (1.37) is equivalent to the solution of the matrix equation

$$\begin{pmatrix} 1 & 0 & 0 & 1 \\ 0 & 1 & \frac{p_c}{2\mathcal{F}^2}\sqrt{\frac{A_0}{A}} - \frac{Q^2}{A^2} & \frac{2Q}{A} \\ 1 & 0 & a & 0 \\ 0 & 1 & 0 & a \end{pmatrix} \begin{pmatrix} \partial_t A \\ \partial_t Q \\ \partial_x A \\ \partial_x Q \end{pmatrix} = \begin{pmatrix} 0 \\ F + \frac{Ap_c}{\mathcal{F}^2 r}\frac{dr}{dx} + \frac{1}{\mathcal{F}^2}\left(\sqrt{\pi A} - \frac{A}{r}\right)\frac{dEW}{dx} \\ d_t A \\ d_t Q \end{pmatrix}$$

Let $c^2 = \frac{p_c}{2\mathcal{F}^2}\sqrt{\frac{A_0}{A}}$ (the squared wave-speed), and $u = \frac{Q}{A}$ (the system velocity), then we can rewrite the above matrix equation as

$$\begin{pmatrix} 1 & 0 & 0 & 1 \\ 0 & 1 & c^2 - u^2 & 2u \\ 0 & 0 & a & -1 \\ 0 & 0 & u^2 - c^2 & a - 2u \end{pmatrix} \begin{pmatrix} \partial_t A \\ \partial_t Q \\ \partial_x A \\ \partial_x Q \end{pmatrix} = \begin{pmatrix} 0 \\ F + \frac{Ap_c}{\mathcal{F}^2 r}\frac{dr}{dx} + \frac{1}{\mathcal{F}^2}\left(\sqrt{\pi A} - \frac{A}{r}\right)\frac{dEW}{dx} \\ d_t A \\ d_t Q - F - \frac{Ap_c}{\mathcal{F}^2 r}\frac{dr}{dx} + \frac{1}{\mathcal{F}^2}\left(\frac{A}{r} - \sqrt{\pi A}\right)\frac{dEW}{dx} \end{pmatrix} \tag{1.38}$$

Non-trivial solutions to the system require that the coefficient matrix is singular, hence the determinant

$$a^2 - 2au + u^2 - c^2$$

must be zero. This is obtained when

$$a = u \pm c = \frac{Q}{A} \pm \sqrt{\frac{p_c}{2\mathcal{F}^2}\sqrt{\frac{A_0}{A}}} \tag{1.39}$$

We will denote the characteristic curve defined by (1.39) having a positive slope by Γ_+ and the one having a negative slope by Γ_-.

The singularity of (1.38) insures the existence of a vector (γ_1, γ_2) such that

$$(\gamma_1, \gamma_2)\begin{pmatrix} u \pm c & -1 \\ u^2 - c^2 & -u \pm c \end{pmatrix} = (0, 0)$$

This vector is given as a multiple of $(1, \frac{1}{-u \pm c})$.

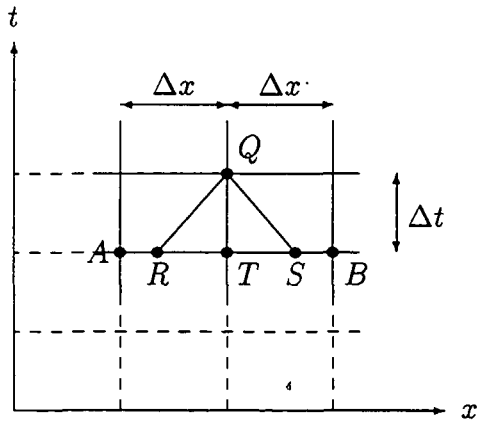

Figure 1.6: The figure shows the points of interest in the specified interval grid.

It is now possible to obtain the following ordinary differential equation along the characteristics

$$\left(1, \frac{1}{-u \pm c}\right) \begin{pmatrix} d_t A \\ d_t Q - F - \frac{A p_c}{\mathcal{F}^2 r}\frac{dr}{dx} + \frac{1}{\mathcal{F}^2}\left(\frac{A}{r} - \sqrt{\pi A}\right)\frac{dEW}{dx} \end{pmatrix} = 0 \quad \Leftrightarrow$$

$$d_t A + \frac{1}{-u \pm c} d_t Q = H^{\pm} \tag{1.40}$$

where

$$H^{+} = \frac{1}{-u+c}\left(F + \frac{A p_c}{\mathcal{F}^2 r}\frac{dr}{dx} - \frac{1}{\mathcal{F}^2}\left(\frac{A}{r} - \sqrt{\pi A}\right)\frac{dEW}{dx}\right)$$

$$H^{-} = \frac{1}{-u-c}\left(F + \frac{A p_c}{\mathcal{F}^2 r}\frac{dr}{dx} - \frac{1}{\mathcal{F}^2}\left(\frac{A}{r} - \sqrt{\pi A}\right)\frac{dEW}{dx}\right)$$

The plus and minus signs corresponds to the positive and negative characteristic, respectively.

1.4.1 Discretization

Using specified intervals, we can now derive a first-order finite difference scheme. In order to do so we will solve the equations on a grid as the one presented in figure 1.6, i.e. on a grid of lines parallel to the axes.

According to the above definitions we are able to obtain a set of difference equations along the characteristics. Locally we approximate the characteristics through the point Q by their tangents. These must intersect the line segments AT and TB respectively in order for the grid to be valid. The points of intersection are, as shown on the figure, R and S, respectively. Hence we approximate the equations in (1.39) and (1.40) by

$$\Gamma_+ : \begin{cases} A_Q - A_R + \frac{1}{-u_R + c_R}(Q_Q - Q_R) = H_R^+ \Delta t \\ x_Q - x_R = (u_R + c_R)\,\Delta t \end{cases} \tag{1.41}$$

$$\Gamma_- : \begin{cases} A_Q - A_S + \frac{1}{-u_S - c_S}(Q_Q - Q_S) &= H_S^- \Delta t \\ x_Q - x_S &= (u_S - c_S)\,\Delta t \end{cases} \tag{1.42}$$

The problem of solving equation (1.12) is thus reduced to the treatment of the above equations.

We assume that the values are known at the points A, B and T and we want to determine u and p at the point Q.

By linear interpolation we get

$$\frac{Q_T - Q_R}{Q_T - Q_A} = \frac{x_T - x_R}{x_T - x_A} = (u_T + c_T)\theta \tag{1.43}$$

where $\theta = \frac{\Delta t}{\Delta x}$. The interpolation condition holds only if $\theta \leq |u \pm c|^{-1}$, which is the CFL-condition. Since we are using linear interpolation the method is first-order correct if the CFL-condition is fulfilled.

We can use the above definition and thereby derive the following equations at the points R:

$$\begin{aligned} Q_R &= Q_T - (Q_T - Q_A)(u_T + c_T)\theta \\ A_R &= A_T - (A_T - A_A)(u_T + c_T)\theta \\ c_R &= c_T - (c_T - c_A)(u_T + c_T)\theta \\ H_R^+ &= H_T^+ - (H_T^+ - H_A^+)(u_T + c_T)\theta \end{aligned}$$

where $\theta = \frac{\Delta t}{\Delta x}$. The corresponding equations at the point S can be derived analogously. Substituting these expressions into the equations (1.41) and (1.42) we can derive expressions for Q_Q and A_Q respectively.

$$\begin{aligned} Q_Q &= \left(\frac{1}{c_R - u_R} + \frac{1}{c_S + u_S}\right)^{-1} \\ &\left(A_R - A_S + \frac{1}{c_R - u_R} Q_R + \frac{1}{c_S + u_S} Q_S + \left(H_R^+ - H_S^-\right)\Delta t\right) \end{aligned} \tag{1.44}$$

and

$$\begin{aligned} A_Q &= (c_R - u_R + c_S + u_S)^{-1} \\ &(Q_R - Q_S + (c_R - u_R)\,A_R + (c_S + u_S)\,A_S + \\ &\left(H_R^+ (c_R - u_R) + H_S^- (c_S + u_S)\right)\Delta t\Big) \end{aligned} \tag{1.45}$$

1.4.2 The boundary conditions

Using this method the values of Q and A can be predicted using the one present characteristic in combination with the specified boundary condition.

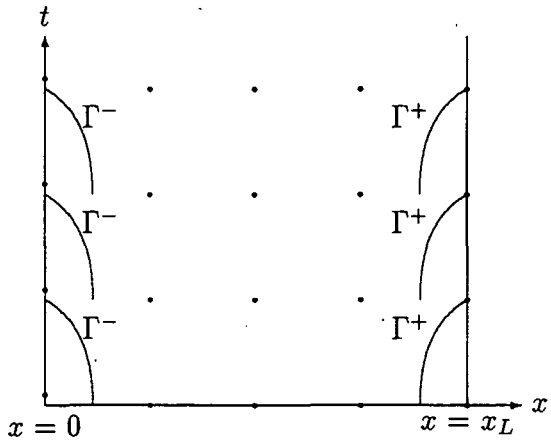

Figure 1.7: On the left boundary $x = 0$ we have only access to the characteristic Γ^-. Analogously we have only access to the the Γ^+ characteristic on the right boundary $x = x_L$

The left boundary $x = 0$

The boundary condition at $x = 0$ is (as in section 1.3.1) given by

$$Q(0,t) = Q_0(t) = (\alpha \sin(\beta t))_{x=0}$$

Also, the dimension less form of this equation is restated here. It is

$$Q_0 = \left(\frac{\alpha}{q} \sin\left(\beta \frac{L^3}{q} t\right)\right)_{x=0}$$

The discretization of the left boundary condition involves only the negative characteristic Γ^-. Therefore, we are dealing with the equations

$$\begin{aligned} x_Q - x_S &= (u_S - c_S)\Delta t \\ A_Q - A_S + \frac{1}{-u_S - c_S}(Q_Q - Q_S) &= H_S^- \Delta t \end{aligned} \tag{1.46}$$

where Q_S, A_S, C_S and H_S^- are calculated as for the interior points. Since we are on the boundary $x = 0$, we already know the value of x_Q. Hence only Q_Q and A_Q are unknowns. We can determine Q_Q directly using the boundary condition.

Combining this result with (1.46) we get the following result for A_Q.

$$A_Q = A_S + \frac{1}{u_S + c_S}(Q_0 - Q_S) + H_S^- \Delta t \tag{1.47}$$

The right boundary $x = x_L$

The boundary condition at $x = x_L$ is also still defined as:

$$Q(x_L, t) = \left(\frac{p - p_e}{R_L}\right)_{x=x_L} = \left(\frac{p_c\left(1 - \sqrt{\frac{A_0}{A}}\right) + p_0 - p_e}{R_L}\right)_{x=x_L}$$

and again, R_L is the peripheral resistance in the end of aorta and p_e is the end capillary pressure. The dimension less version of this equation is similar, but contains the corresponding non-dimensional quantities.

The discretization of the right boundary condition involves only the positive characteristic Γ^+, and this case is treated analogously to the left boundary condition.

$$\begin{aligned} x_Q - x_R &= (u_R + c_R)\Delta t \\ A_Q - A_R + \frac{1}{-u_R + c_R}(Q_Q - Q_R) &= H_R^+ \Delta t \end{aligned} \tag{1.48}$$

where Q_R, A_R, C_R and H_R^+ are calculated as for the interior points. Since we are on the boundary $x = x_L$ we already know the value of x_Q.

Again, we can calculate the unknowns Q_Q and A_Q using (1.48) and the boundary condition.

$$Q_Q = \frac{(p_c)_Q\left(1 - \sqrt{\frac{(A_0)_Q}{A_Q}}\right) + p_0 - p_e}{R_L} \tag{1.49}$$

For A_Q we then get

$$\begin{aligned} 0 &= A_Q - A_R + \frac{(p_c)_Q\left(1 - \sqrt{\frac{(A_0)_Q}{A_Q}}\right) + p_0 - p_e - R_L Q_R}{R_L(-u_R + c_R)} - H_R^+ \Delta t \\ &= \sqrt{A_Q^3} + \sqrt{A_Q}\left(\frac{(p_c)_Q + p_0 - p_e - R_L Q_R}{R_L(-u_R + c_R)} - A_R - H_R^+ \Delta t\right) \\ &\quad - \frac{(p_c)_Q\sqrt{(A_0)_Q}}{R_L(-u_R + c_R)} \end{aligned}$$

This is a cubic equation in $\sqrt{A_Q}$.

If we let $x = \sqrt{A_Q}$, we can rewrite the above equation as

$$f = x^3 + Bx + C$$

Again we can estimate the root using Newton's method. The only difference to the description on page 21 is that in this case we are only dealing with one equation.

In this case the first-order scheme looks like

$$x_{i+1} = x_i - f'(x_i)^{-1} f(x_i)$$

where i still refers to the number of iterations. In this case the Jacobian simply becomes the usual derivative of f. The initial guess for x_0 is chosen as

$$x_0 = \sqrt{A((N-1)\Delta x)}$$

which is the the last predicted value of $\sqrt{A}$ at the time level where the root $\sqrt{A_Q} = \sqrt{A(N\Delta x)}$ should be found. If A does not change too rapidly, this value should be rather close to the wanted root.

Chapter 2

Convergence of the two methods

In order to test the convergence of the two methods, we have applied a known solution $(x+t+1)$ to A and Q, respectively. Using this knowledge we have modified the right hand side of the systems (1.12) and (1.14) and the boundary conditions in order for the equations to be consistent.

Substituting the solution into (1.12) results in:

$$\frac{\partial}{\partial t}\begin{pmatrix} A \\ Q \end{pmatrix} + \begin{pmatrix} 0 & 1 \\ \frac{p_c}{2\mathcal{F}^2}\sqrt{\frac{A_0}{A}} - \frac{Q^2}{A^2} & \frac{2Q}{A} \end{pmatrix} \frac{\partial}{\partial x}\begin{pmatrix} A \\ Q \end{pmatrix} = \begin{pmatrix} \cdot & 2 \\ 2 + \frac{p_c}{2\mathcal{F}^2}\sqrt{\frac{A_0}{x+t+1}} \end{pmatrix}$$

The result from the conservative system (1.14) is:

$$\frac{\partial}{\partial t}\begin{pmatrix} A \\ Q \end{pmatrix} + \frac{\partial}{\partial x}\begin{pmatrix} Q \\ \frac{Q^2}{A} + \frac{A_0 p_c}{\mathcal{F}^2(1-p_E)} \end{pmatrix} = \begin{pmatrix} 2 \\ 2 + \frac{p_c}{2\mathcal{F}^2}\sqrt{\frac{A_0}{x+t+1}} + \frac{\sqrt{\pi(x+t+1)}}{\mathcal{F}^2}\frac{dEW}{dx} \end{pmatrix}$$

For both systems the corresponding boundary conditions are given by

$$\begin{aligned} A(0,t) &= Q(0,t) = t+1 \\ A(L,t) &= Q(L,t) = t+2 \end{aligned}$$

and the initial condition is

$$A(x,0) = Q(x,0) = x+1$$

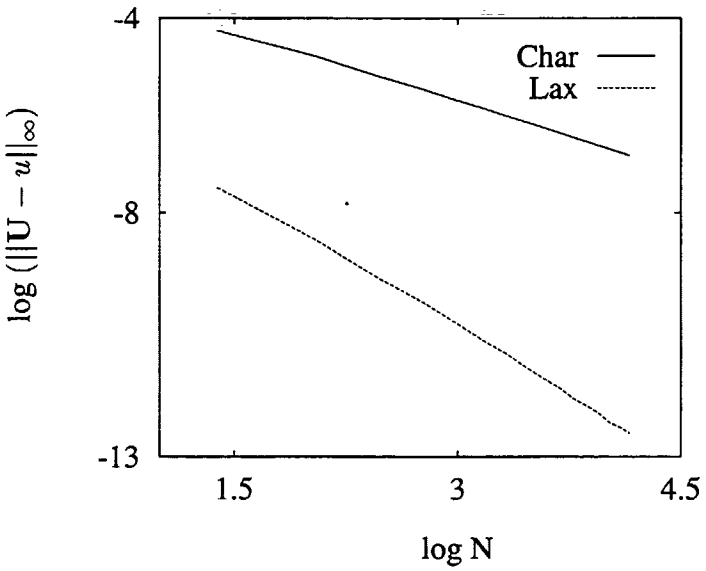

Figure 2.1: The convergence rate (n) for Lax Wendroff's two-step method and the method of characteristics. For Lax Wendroff's method $n \approx 2$ and $\log c \approx -4.5$, for the method of characteristics $n \approx 1$ and $\log c \approx -3$.

In these experiments we have used the infinity norm to determine the rate of convergence. Let $\mathbf{U}$ determine the approximate computed solution, and $\mathbf{u}$ the exact solution. Further, let h be the size of the space step and N the number of steps in the interval zero to one, which covers the entire domain, since the equations are dimension less.

Assume that $||\mathbf{U} - \mathbf{u}||_\infty$ is $\mathcal{O}(h^n)$. Then

$$\begin{aligned} ||\mathbf{U} - \mathbf{u}||_\infty &\leq ch^n = c\left(\frac{1}{N}\right)^n \quad \Leftrightarrow \\ \log\left(||\mathbf{U} - \mathbf{u}||_\infty\right) &= \log c - n \log N \end{aligned}$$

where c is some positive constant.

The order of convergence n can then be read of the graphs as the negative slope of $\log ||\mathbf{U} - \mathbf{u}||_\infty$ as a function of $\log N$. Further, the constant c can be determined from the intersection of the graph with the line $x = 1$. As shown in figure 2.1, $n \approx 1$ for the method of characteristics, and $n \approx 2$ asymptotically for Lax Wendroff's two step method. This is also the values that are expected since the method of characteristics is supposed to be of first-order and Lax Wendroff's method is a second-order method.

Chapter 3

Results

In this section we will present some results from both methods. One important concern is an investigation of the behavior of the outflow resistance R_L, since the results are (as we will see) very sensitive to this parameter. Also the the amount of tapering influences the solution.

The equations solved are the ones given in (1.20) for Lax Wendroff's two step method, and (1.44) and (1.45), for the method of characteristics. The boundary conditions are given as described in (1.21) and (1.23). The initial conditions are chosen so that the flow $Q(x,0) = 0$ and the cross-sectional area $A(x,0) = A_0$ (the cross-sectional area at pressure $p = p_0$).

The default numerical parameters and the default values of the input parameters are stated below.

The default numeric parameters		
N	64	Number of lattice points in the x direction.
h	$\frac{1}{N}$	The interval length of Δx.
k		The interval length of Δt. This is determined as large as possible within the bounds of the CFL-condition.
finaltime		The end-simulation time.

The default input parameters			
ρ	1.06	$g\ cm^{-3}$	The density of the blood ([3] page 231)
μ	0.049	$poise$	The viscosity of the blood. ([3] page 231)
L	76	cm	The length of aorta. (Empirical data)
p_0	760	$mmHg$	The pressure of the surroundings.
r_{top}	1.25	cm	The radius at the top of aorta. (Empirical data)
r_{bot}	1.00	cm	The radius at the end of aorta. (Empirical data)
D	0.2	cm	The wall thickness of aorta. (Empirical data)
E	3.8510^6	$mmHg$	Young's modulus ([21])
p_e	25.0	$mmHg$	The end capillary pressure - relative to the surroundings. ([2] page 22)
R_L	0.95	$cm^3 s^{-1} mmHg$	The peripheral resistance of aorta. ([1] page 273)
Q_0	733		The amplitude of the input flow corresponding to a stroke volume of 70 cm^3. ([2] page 22)
k	25		The multiplication factor used when the friction is determined, ([3] page 225)
T_{per}	0.8	s	The period of one heart cycle. ([2] page 22).

In the first run (see figure 3.1) we have computed the relative blood pressure as a function of time and space. In this run the default parameters are used. As shown in the figure, the method of characteristics (graph A) shows a slight upward deflection in the right boundary. In general, the method of characteristics gives rise to a slightly higher pressure than does the Lax Wendroff method (graph B). Further, it is evident that the value of $R_L = 0.95$ used in the current prototype simulator is too high. This is evident since the pressure rises in the right boundary, and hence the reflected wave is too extreme. The parameter used in the current simulator is a lumped parameter consisting of the peripheral resistance for the entire arterial system. However, this value of R_L can possibly have other effects when the bifurcations of the system are taken into account.

This pressure rise also causes large reflections as time increases. If one instead lowers the value of R_L as far down as 0.2 or even 0.1 (see figure 3.2) the reflection damps out rather fast. Since the results are more smooth, the method of characteristics (graph A and C) is adequate, and it is hard to distinguish between this and the results from Lax Wendroff's method (graph B and D). However, viewing a two-dimensional graph displaying the pressure as a function of time (in the case $R_L = 0.2$) over a number of periods, it is clear that the results becomes stable after a few periods (see figure 3.3). These results are valid both using the method of characteristic (graph A) and Lax Wendroff's method (graph B). We therefore tend to believe, that the deviation between the two methods is due to the fact, that the method of characteristics is a first-order method, while Lax Wendroff's two step method is of second-order.

Another concern is the amount of tapering in the system. In the results stated, the radius of aorta varies from 1.25 cm. to 1.00 cm. which admittedly is very little compared to the tapering of the entire arterial system. However, in the human aorta the tapering between the top of aorta and the iliac bifurcation is approximately as stated above. What happens when the tube is tapered further is that the pressure increases along the aorta, and the reflection wave is returned faster. These phenomena are seen on the graphs in figure 3.4. All the results are made keeping the radius at the top of aorta unaltered (1.25 cm.). Also, the peripheral resistance is the same ($R_L = 0.4$). In graph A of figure 3.4 the aorta is tapering as in the previous runs, in B the radius at the bottom of aorta is 1.00 cm., in C it is 0.75 cm., and in D it is 0.50 cm.

Evaluating the results as a whole is complicated, since so many different factors play important roles. If one for instance considers figure 3.3, it is hard to determine whether the reflections could be the dicrotic notch, or merely a numerical artifact. Looking at the graphs in figure 3.5, one can see that the further we get down the aorta the closer the reflecting wave comes to the original pulse wave, and then after a certain point they separate again. If all the branches of the system were present they would probably all cause similar phenomena supporting the conjecture that the dicrotic notch is due to the reflection stemming from the resistance in the far boundary. Further we wish to observe an increase in the pressures throughout the aorta. This is certainly present, but it depends a lot on the amount of tapering (as seen in figure 3.4). In general, we must conclude that it is hard to compare these results with the reality, since the bifurcations remain to be taken into account.

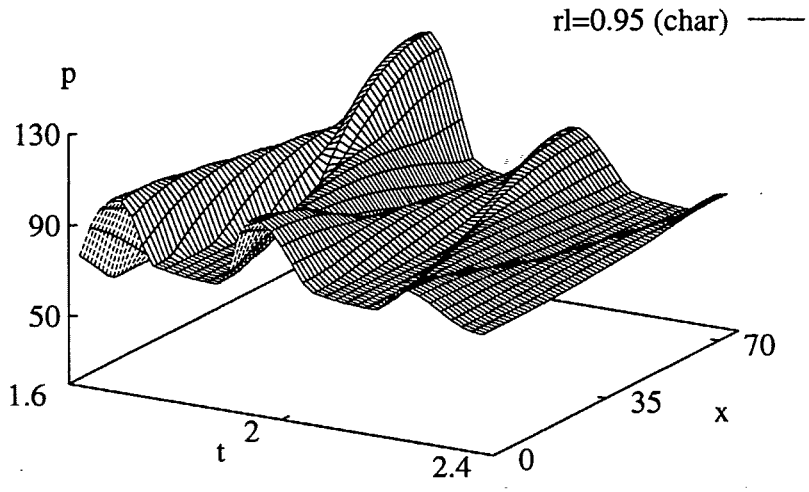

A

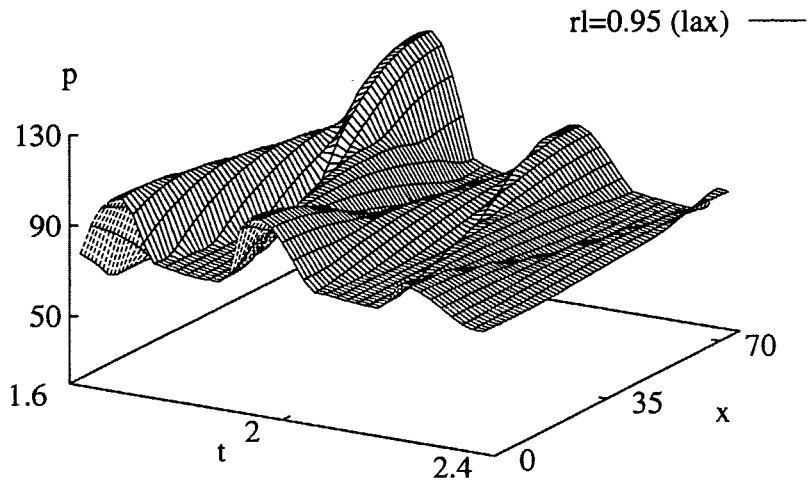

B

Figure 3.1: The pressure as a function of time and space. The plots cover both the method of characteristics (graph A) and Lax Wendroff's method (graph B). The peripheral resistance is in this case 0.95 which is the value used in the current simulator. However, this is a lumped value representing the entire arterial system, and it has therefore no meaning in this example where no bifurcations are taken into account.

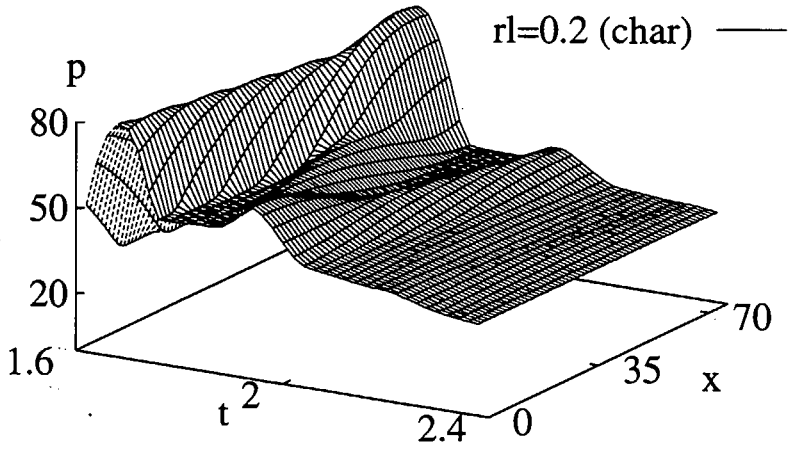
rl=0.2 (char)
p
80
50
20
1.6
t
2
2.4
0
35
x
70

A

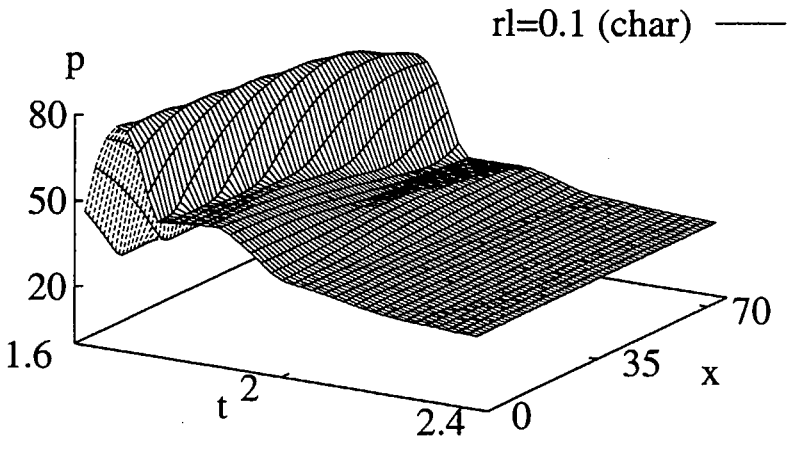
rl=0.1 (char)
p
80
50
20
1.6
t
2
2.4
0
35
x
70

B

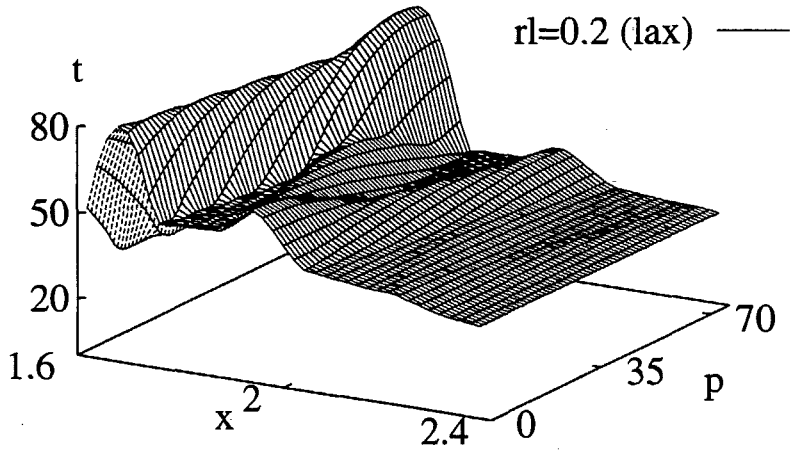

C

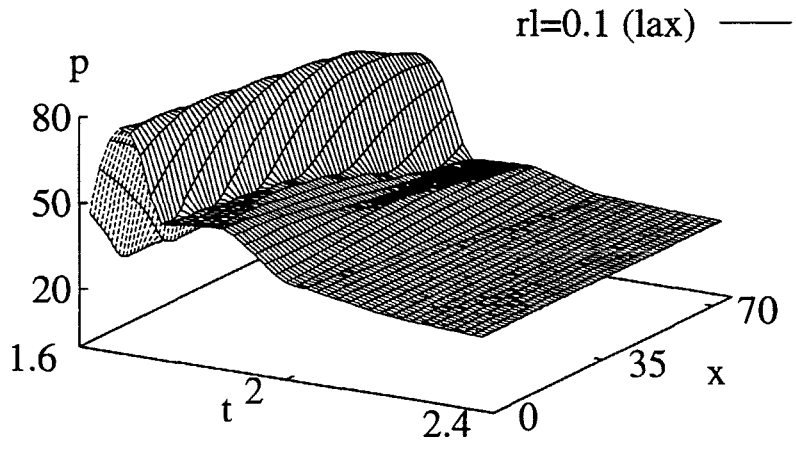

D

Figure 3.2: The pressure as a function of time and space. In this case R_L has the values of 0.2 and 0.1 respectively. Results from both the method of characteristics (char) and Lax Wendroff's two-step method are depicted.

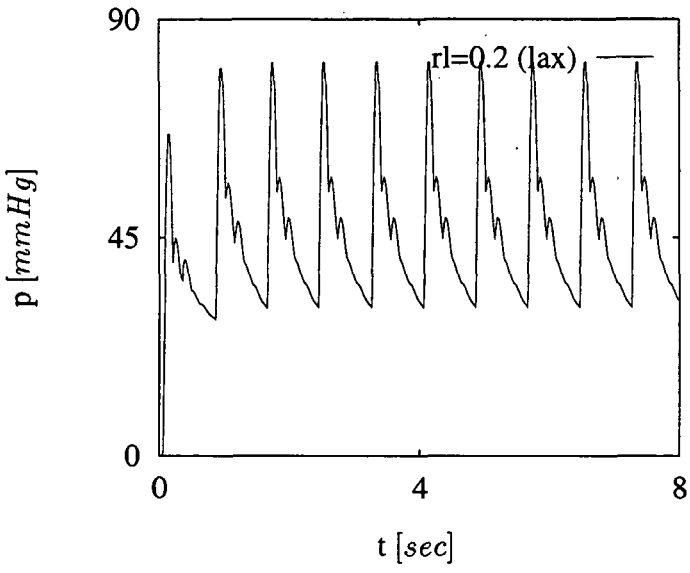

Figure 3.3: The pressure as a function of time in the middle of aorta. In this case only Lax Wendroff's method is considered, but the method of characteristics shows the same phenomenon, namely that the solutions becomes stable after only one period. The first period shows a pressure that is too low, and this phenomenon is due to the fact that the chosen initial condition is not correct.

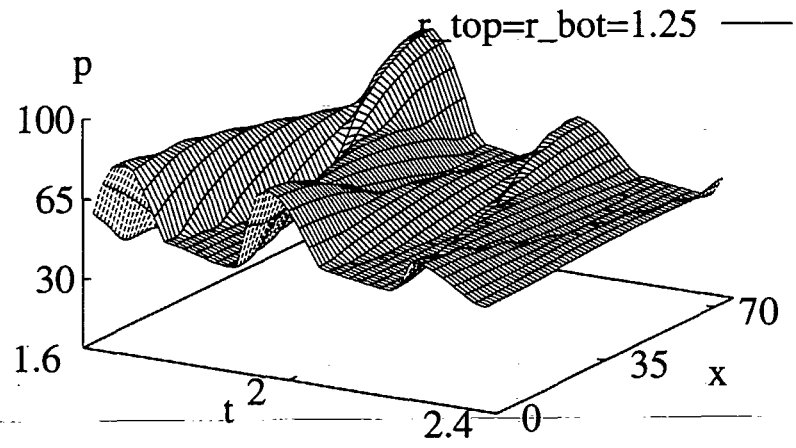
r_top=r_bot=1.25
p
100
65
30
1.6
t
2
2.4
0
35
70
x

A

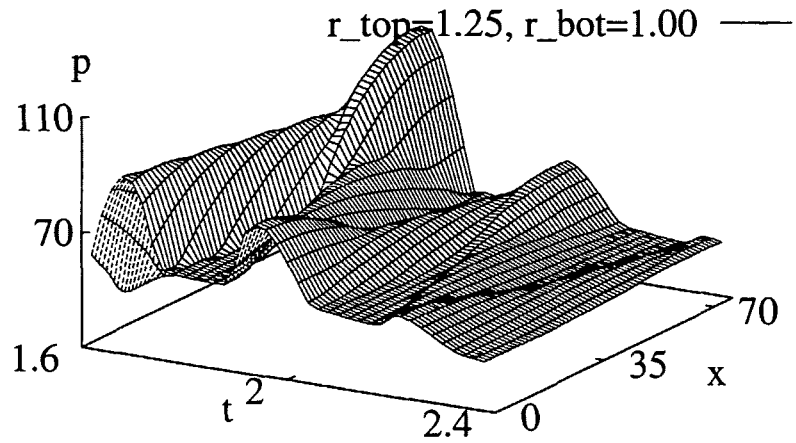
r_top=1.25, r_bot=1.00
p
110
70
1.6
t
2
2.4
0
35
70
x

B

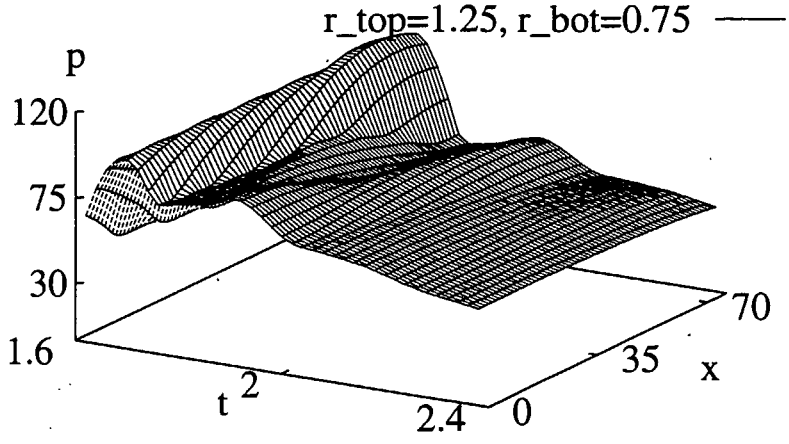

C

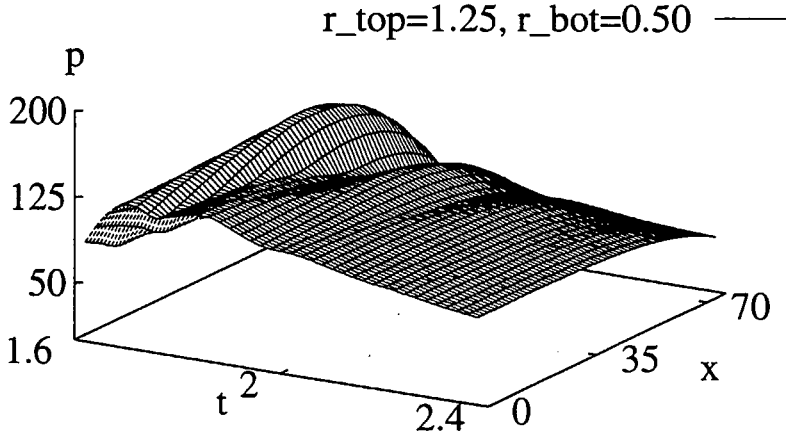

D

Figure 3.4: When the tapering of the tube is increased the pressure rises and the reflection wave becomes faster. In all four runs only Lax Wendroff's two-step method has been used.

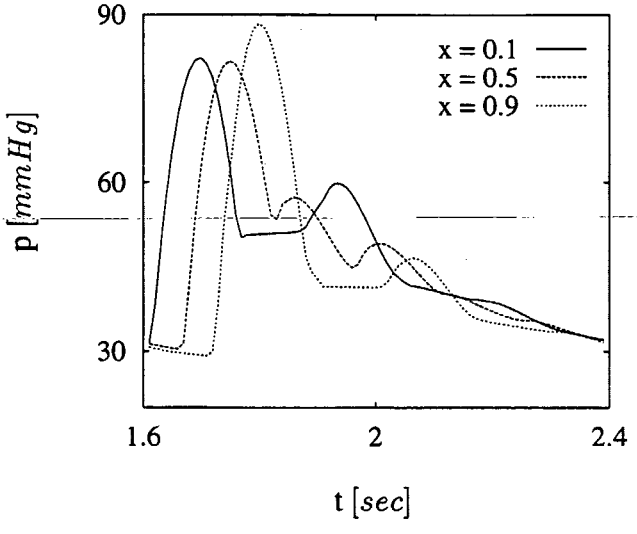

Figure 3.5: The pressure as a function of time at three different positions in aorta: halfway down, 10% down and 90% down. Notice that the first reflection wave is approaching the original pulse wave the closer we get to the bottom of aorta. Only Lax Wendroff's method is considered, but the method of characteristics shows the same behavior.

Chapter 4

Timing of the two methods

In order to estimate the efficiency of, and compare, the two methods, we have made several runs using a number of computers spanning from personal computers (a pentium 90MHz with 512 bytes cache and a 486DX2-66 having no cache) to some workstations (a HP9000-735, a DEC-station 5000/120 and an IBM RISC 6000/250). On all computers, the program was executed under UNIX and, except on the IBM machine, it was compiled using gnu c++. All runs simulated three periods corresponding to a model time of 2.4 sec. The results show that it is certainly possible to run the simulation in real time (except in the cases where the grid is refined extensively). Further, it is seen that Lax Wendroff's method is faster than the method of characteristics. The results of these runs are displayed in the table below.

Platform	N	CPU-time (Lax)	CPU-time (Char)
486DX2-66 (no cache)	32	0:10	0:15
Linux 1.0,	64	0:33	0:54
gcc 2.5.8 (-O2)	128	2:07	3:26
	256	8:14	13:10
DEC-station 5000/120	32	0:08	0:13
fatou.ruc.dk	64	0:27	0:50
gcc 2.6.0 (-02)	128	1:42	3:13
	256	6:44	12:26
Pentium-90	32	0:03	0:05
(512Kb cache)	64	0:10	0:18
Linux 1.1.47,	128	0:39	1:18
gcc 2.2.5 (-02)	256	2:32	4:38
Hp9000 735	32	0:01	0:02
tyr.diku.dk	64	0:04	0:08
gcc 2.5.8 (-02)	128	0:18	0:29
	256	1:06	1:50

IBM system 6000/250	32	0:01	0:02
pauli.ruc.dk	64	0:04	0:07
xlC 1.3.0.0	128	0:14	0:26
	256	0:55	1:41

Chapter 5

The outflow due to the branching of the system

As shown in figure 1.1 it is obvious that the model used uptil now doesn't match the system that we try to model. It is insufficient since it doesn't include anything dealing with the many branches of the system. At each branch some of the blood leaves the system. This outflow concerns both the major branches shown in the figure and a number of smaller branches not included. There are several possibilities to treat these outflows. In this section we will concentrate on the outflow along the aorta, and we will deal explicitly with the outflow conditions at the iliac bifurcation.

The outflow along the aorta can be treated from two different points of view. The first concerns a treatment of the outflow as a continuous function in space, while the second models the outflow at the various bifurcations as discrete points. The continuous approach adds an outflow condition to the right hand side of the continuity equation (1.2), hence

$$\frac{\partial A}{\partial t} + \frac{\partial Q}{\partial x} = -\Psi$$

The outflow is contained in the function Ψ which is dependent on the position in aorta and the corresponding pressure.

This function could be determined as described by Anliker[3], where Ψ is a global function that assembles all outflows along the aorta (see figure 5.1B). The function is given by

$$\Psi(p,x) = \begin{cases} \gamma(p-p_c)\left(1.1 + \cos\left(\frac{5\pi}{2}\frac{x}{x^*}\right)\right) & \text{for } x \leq x^*(=70cm.) \\ \gamma(p-p_c)\,1.1\,e^{-0.08(x-x^*)} & \text{for } x > x^* \end{cases} \tag{5.1}$$

In the paper, it does not appear why this particular function was chosen, but it does not seem to be physiologically founded.

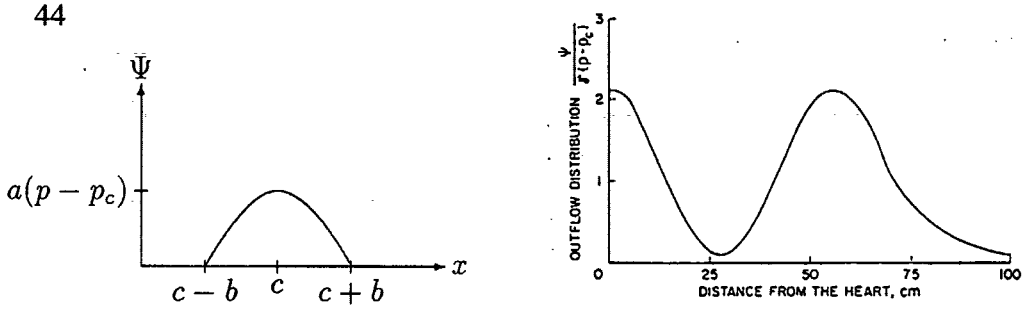

A B

Figure 5.1: The localized outflow condition is shown in A and the general outflow seepage used by Anliker[3] is shown in B. In B outflow distribution of blood through the arterial wall is defined by equation (5.1).

Since the outflow occurs at branches along the aorta, another approach is to make the outflow condition local in the neighborhood of each bifurcation. Assume that there are k branches along the aorta. The outflow at the k'th bifurcation could then be defined to be proportional to

$$\Psi_k(p,x) = \begin{cases} (p-p_c)\left(\frac{\cos\left(\frac{\pi}{b_k}(x-c_k)\right)+1.0}{2}\right)^2 & \text{for } x \in [c_k - b_k; c_k + b_k] \\ 0 & \text{otherwise} \end{cases}$$

where the bifurcation is centered at c_k and has the width $2b_k$, and the actual proportionality factor depends on the size of the bifurcation (see figure 5.1A).

The total outflow along the aorta will then be given by

$$\Psi(p,x) = \sum_{k=1}^{N} a_k \Psi_k(p,x)$$

where the coefficients a_k must be determined as follows:

The fraction of blood (CO_f) leaving through the branch centered at c_k is

$$\int_{c_k-b_k}^{c_k+b_k} a_k \Psi_k(p,x)dx = CO_f$$

Since CO_f can be measured, it is possible to determine a_k by

$$a_k = \frac{CO_f}{\int_{c_k-b_k}^{c_k+b_k} \Psi_k(p,x)dx}$$

when $x \in [c_k - b_k; c_k + b_k]$.

Another way to treat the outflow is by decomposing the aorta into a number of independent pieces, each having no branches. These should then be joined together at the bifurcation. In this case each piece is treated separately, and all branches can be regarded as discrete points. At each end of the tube piece one should consider a boundary condition and some specifications linking the two pieces of the tube together.

The advantage of the first approach is the possibility to treat the entire flow along the aorta by one set of equations. The disadvantage is the necessity to include a large number of grid points in order to capture the localized outflow at the branches. However, such a grid may be too fine grained for the bulk of the tube piece, but it is possible to use graded grids, and thereby only use the fine grained grids in the sections close to the bifurcation. In the paper by Anliker[3] these considerations are not discussed even though this would have been very useful. In fact he does not discuss his choice of outflow condition at all. Due to this problem and the fact that the global outflow condition presented by Anliker[3] is not physiologically based, we have chosen to concentrate on the piecewise approach.

The outflow stemming from the aorta can be divided into two groups: The first deals with the outflow along the aorta, where the point of interest is the pressure and the flow in the aorta before and after a particular bifurcation. This is the situation displayed in part A and B of figure 5.2. The second type is found at the iliac bifurcation located at the bottom of aorta. In this case the tube splits into two minor tubes of comparable size, and we are interested in the flow and pressure in both of these. This is the situation illustrated in figure 5.2.C. If one is interested in finding the pressure and the flow in the radial artery, this can be treated as the case illustrated in figure 5.2.A and B. Instead of letting the outflow condition be determined at the top, we let $Q^{(3)}$ and $Q^{(2)}$ switch role, and the boundary condition $\frac{p^{(3)}-p_e}{R^{(3)}}$ should be assigned to the lower part of aorta. In the following we will sketch how the bifurcations can be treated.

The exact modeling of the bifurcations can be discussed further, and we will introduce two different approaches. One way of attacking the problem is to use the approach suggested by Stettler[25], where a separate segment containing the branch is introduced (see figure 5.2.A). Within this segment the tube is assumed to taper linearly (as opposed to the exponential tapering in the bulk of the arteries). In order to predict the flow and the pressure across such a segment, the following conditions are applied: First, we assume that the flow is continuous over the segment, hence

$$Q^{(1)} = Q^{(2)} + Q^{(3)} + \frac{d}{dt}\int_{x_1}^{x_2} A\, dx \tag{5.2}$$

Second, we apply Bernoulli's relation

$$p^{(1)} - p^{(j)} = \frac{\rho}{2}((u^{(j)})^2 - (u^{(1)})^2) + \rho\int_{x_1}^{x_2} \frac{\partial u}{\partial t}\, ds + \Delta p^{(j)} \tag{5.3}$$

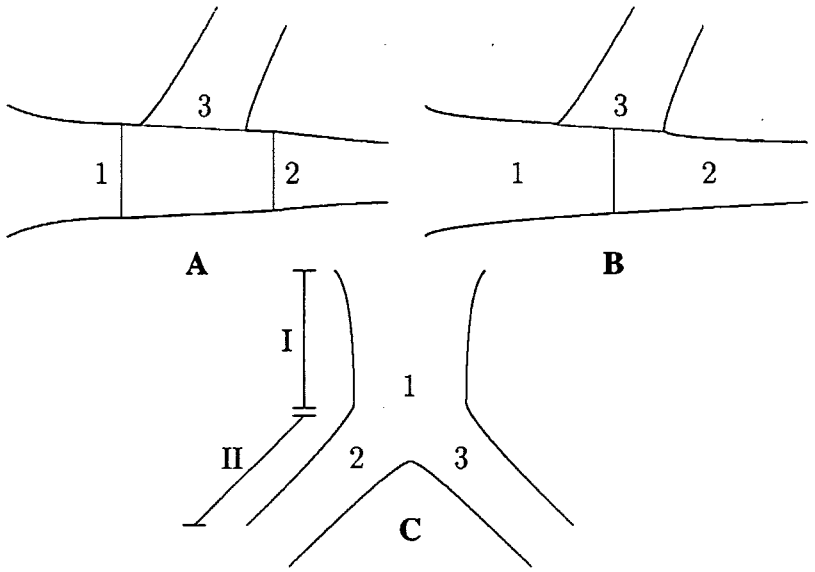

Figure 5.2: A sketch of the different kinds of branching systems. In A the bifurcation is modeled using a separate segment, in B the outflow is determined as a point, and in C the iliac bifurcation is showed.

where $j = 2, 3$.

$$\Delta p^{(j)} = \lambda^{(j)} \frac{L}{4R^{(j)}} \frac{Q}{A}$$

reflects the curvature of the branching vessel as well as the friction loss due to viscosity.

$$\lambda^{(j)} = \begin{cases} 0.37 \left(\frac{1}{2} Re^{(j)} \sqrt{\frac{R^{(j)}}{r^{(j)}}} \right) \left(0.36 \frac{64}{Re^{(j)}} \right) & \text{for } Re^{(j)} \sqrt{\frac{R^{(j)}}{r^{(j)}}} > 10^{1.6} \\ \frac{64}{Re^{(j)}} & \text{for } Re^{(j)} \sqrt{\frac{R^{(j)}}{r^{(j)}}} < 10^{1.6} \end{cases}$$

and finally $Re^{(j)} = \frac{2R^{(j)} \rho v_1}{\mu}$ and $R^{(j)}$ is the radius of curvature of the branching vessel. The subscripts refer to the numbers shown in figure 5.2. However, as demonstrated by Lighthill[6], the error in assuming that the total flow into a bifurcation equals the outflow, and that the pressure is continuous can be estimated by regarding the magnitude of the rate of change of the pressure over a bifurcation using a linearized model. For a bifurcation such as the iliac where the dimension of the branches is of order 1 cm., the error is approximately one percent, so it makes sense to regard the bifurcation as a point over which the pressure and flow are continuous (see figure 5.2.B). Hence, we are left with the conditions:

$$Q^{(1)} = Q^{(2)} + Q^{(3)} \quad \text{and} \quad p^{(1)} = p^{(2)} = p^{(3)} \tag{5.4}$$

Assuming that the flow in the two branches of the iliac bifurcation are equal ($Q^{(2)} = Q^{(3)}$, and hence $Q^{(1)} = 2Q^{(2)}$), only one of them needs to be determined. One difference

between the two cases (A, B versus C) is that the flow in C deflects when moving from 1 to 2, whereas the flow in A has the same direction before and after the bifurcation. Another difference is that in A and B the rate of change of the cross-sectional area is smooth in the transition from 1 to 2: The aorta keeps on tapering with the same rate. In C the cross-sectional area is discontinuous at the splitting point. However, if one allows discontinuities in the cross-sectional area, and disregards the angle between I and II in C, the two situations can be treated using the same set of equations.

In appendix A the bifurcation is modeled using the assumption that it happens at a point, i.e. equations in (5.4) should be applied. In appendix B the approach of using a separate bifurcation segment is used, hence the equations (5.2) and (5.3) should be applied. The conditions linking two tube pieces together at some bifurcation are obtained using conservation of mass and Bernoulli's relation. Further, one must determine boundary conditions for the right hand side of tube 1 and the left hand side of tube 2. The mathematical description (which is rather technical) of this is done in the appendices A and B. The idea follows the same approach used in section 1.3.2 where the boundary condition concerning the right boundary at the bottom of the aorta is treated, and the numerical treatment will be based on Richtmayer's version of Lax Wendroff's two step method.

5.1 The boundary conditions

The boundary condition that ensures a reasonable cardiac ejection rate at the proximal end of the aorta is analogous to the one given in section 1.3.1.

At the bifurcation point (in the case where we do not know the relationship between $Q^{(2)}$ and $Q^{(3)}$) and at the bottom of the arteries the condition stated in section 1.3.2 will be used again.

However, due to its problems another approach is suggested by Anliker[2] and Stettler[24]: Here the total outflow is

$$Q^{(3)} = R_p(p^{(1)} - p_e)(A^{(3)})^2 + R_q Q^{(1)} \tag{5.5}$$

where R_p and R_q are lumped parameters. The first term represents outflow from relatively small rigid branches perpendicular to the main conduit, and consequently the outflow is assumed to be proportional to a Poiseuille flow. The second term represents outflow from a branch into two symmetrical vessels. Equation (5.5) can be validated empirically, but it is not possible to establish it from the physical theory. Because the outflow in general depends on both $Q^{(1)}$ and $p^{(1)}$ one may argue in favour of the linear relationship in (5.5).

Since we concentrate on boundary conditions that can be either derived from the theory or empirically established, we have still chosen to focus on the simple condition stated

in section 1.3.2, knowing that this condition does not mathematically quite fulfill the demands described above.

5.2 Model evaluation and results

As stated above the equations including the iliac bifurcation are solved numerically using Lax Wendroff's two step method, Peskin[17]. In order to be able to compare the branching model to the results presented in section 1.3 we carry out simulations of two systems: System 1 consists only of the aorta (part I in figure 5.2.C) while system 2 comprises both the aorta, the iliac bifurcation and one of the femoral arteries viewed as a symmetrical bifurcation point (parts I and II in figure 5.2.C). Note that the boundary condition using the peripheral resistance R_L is in both cases applied only once, namely at the right boundary. However, when comparing R_L from the two systems we get the relation $R_L^{(1)} \approx \frac{R_L^{(2)}}{2}$ where $R_L^{(1)}$ and $R_L^{(2)}$ are the resistances in system 1 and 2, respectively.

As seen in figure 5.3 and 5.4 both systems show an increase of pressure along the aorta (in figure 5.4 the aorta is the part between $x = 0$ cm. and $x = 42.5$ cm.). Both systems also show an increase in the steepness of the pressure profiles along the aorta. However, this is difficult to see on the 3D plots presented. In the physiological situation it is also possible to detect a dicrotic notch and as indicated in figures 5.3 and 5.4 this is due to the reflections in the system, which in turn are consequences of the tapering of the vessels. It is seen that introduction of the bifurcation does not change these phenomena and we therefore conclude that our model shows the right qualitative behavior.

Figures 5.5.A and B show a plot of $p(x_L, t)$, where x_L is at the bottom of aorta, for a number of peripheral resistances. In both cases the pressure increases with increased resistance, but in case of system 1, where no bifurcations are taken into account, the reflections become more evident and also reflections of higher order appear as R_L is increased which in turn causes a large disturbance of the pressure profile. Finally, figure 5.5.C shows the systolic and diastolic pressures as a function of the peripheral resistance (the two top lines concern the systolic pressure and the two bottom lines the diastolic pressure). Also, in this figure it is possible to detect a more stable increase of $p(x_L, t)$ with increasing R_L.

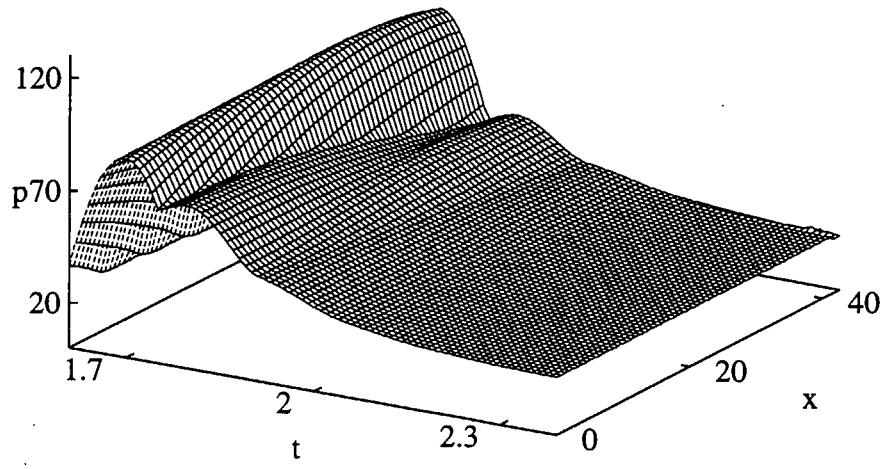

Figure 5.3: The pressure in aorta as a function of time and space.

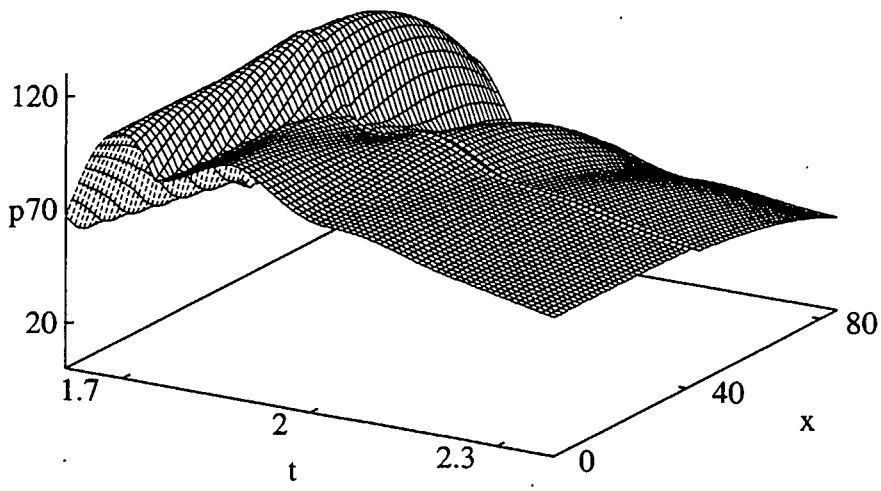

Figure 5.4: The pressure in aorta ($x \leq 42.5$ cm.) and in part of the femoral arteries ($x > 42.5$ cm.) as a function of time and space.

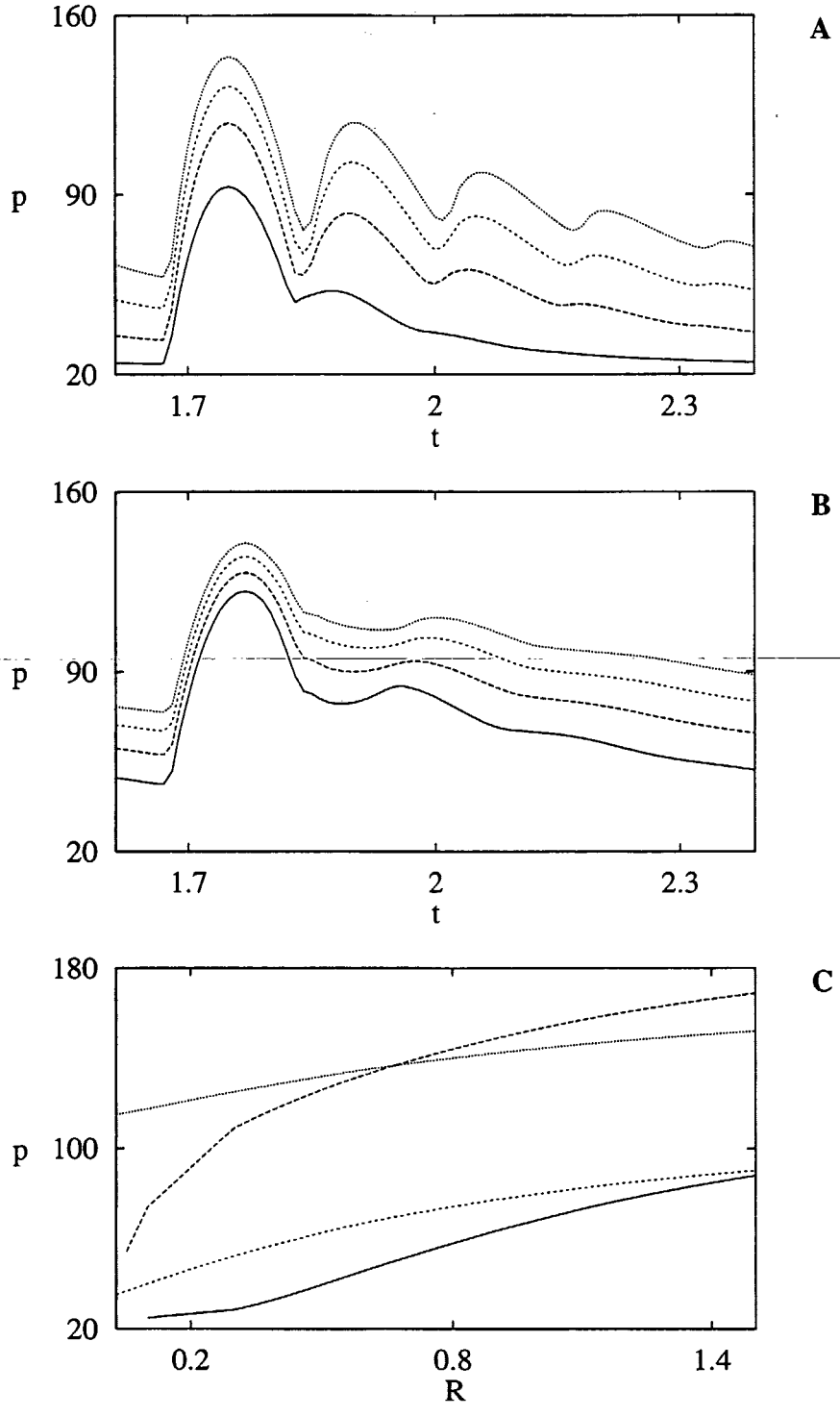

Figure 5.5: **A** and **B** show the pressure as a function time for four values of R_L. Since a symmetrical bifurcation is the value of R_L in **A** equals $\frac{R_L}{2}$ in **B**. In **C** the systolic and diastolic pressures are plotted as functions of R_L for system 1 and 2, respectively.

Chapter 6

Conclusion

As expected the method of characteristics is not as reliable as Lax Wendroff's two-step method. It is generally not a good idea to start out using the method of characteristics, and thereafter manipulating it to obtain a finite difference method. These manipulations require more considerations and increase the computation time, as shown in the previous section. Another thing that makes Lax Wendroff's method superior is the fact that it is second-order correct. According to Ralston[7] it is, however, possible to develop a second-order scheme also for the method of characteristics, but using this approach the method will no longer be explicit, and the required computing time will therefore increase even more. Another drawback is that the second-order method of characteristics becomes considerably more complicated. Therefore the work in this report has verified that it is best to use Lax Wendroff's two-step method in this particular project – both with respect to accuracy and speed.

Further we can conclude that the system is rather sensible to the peripheral resistance (as shown in the results in figure 3.4). Therefore results from inclusion of bifurcations (e.g. the iliac bifurcation) should focus on this dependency. Due to the argument presented by Lighthill[6] we will concentrate on the approach that concerns the bifurcation at a point as shown in figure 5.2.B and derived in detail in appendix A.

The most important point is the qualitative effect of moving the boundary condition to the Femoral arteries. The fact that the pressure profiles in aorta are more stable when the boundary condition is placed after the iliac bifurcation, confirms the point stated by Peskin[17] that the flow and pressure are proportional only when far away from the heart. We will therefore conclude that if a suitable boundary condition should be applied (in system 1) at the bottom of aorta, the peripheral resistance should be a function of time. However, since this can be a difficult task, it is more reasonable – and also adequate – to include at least one of the major bifurcations in order to work with the boundary condition suggested in (1.3.2).

Another point we want to consider is the range of pressures in system 1. The current choice of parameters seems to create an excessive gap between the systolic a diastolic

pressures. In the case of system 2 with $R_L = 0.5$ this gap becomes more reasonable, and we believe that this situation could be improved further through slight changes in the geometry.

These studies have been very useful to our work in estimating the level of detail needed in order to construct an adequate model for the arterial system and we conclude that trying to lump everything into one single tapered tube is not feasible

Appendix A

A discrete outflow determined at a single point

In this section we will develop the equations necessary for treating a bifurcation as displayed in figure 5.2.B. First of all, assume that the flow is conserved, hence

$$Q^{(1)}(L,t) - Q^{(2)}(L,t) = Q^{(3)}(L,t) = \frac{p^{(3)}(L,t)}{R^{(3)}(L,t)} \tag{A.1}$$

and, secondly assume, that the pressure is continuous across the bifurcation. Hence

$$p^{(1)}(L,t) \;=\; p^{(2)}(L,t) = p^{(3)}$$

According to Lighthill[6] page 233 these assumptions should be adequate. The latter condition results in the additional requirement that

$$p_c^{(1)}\left(1 - \sqrt{\frac{A_0^{(1)}}{A^{(1)}}}\right) = p_c^{(2)}\left(1 - \sqrt{\frac{A_0^{(2)}}{A^{(2)}}}\right) = p_c^{(3)}\left(1 - \sqrt{\frac{A_0^{(3)}}{A^{(3)}}}\right) \tag{A.2}$$

This fact is due to the state equation defined in (1.5). The superscripts (1) and (2) refers to the two parts of the tube as displayed in figure 5.2.

Seen from the first part of the tube (1), the equations at the points on the right boundary are

$$\begin{aligned}(Q^{(1)})_L^{n+1} \;=\; & (Q^{(1)})_L^n - \frac{k}{h}\left(\left(R_2^{(1)}\right)_{L+\frac{1}{2}}^{n+\frac{1}{2}} - \left(R_2^{(1)}\right)_{L-\frac{1}{2}}^{n+\frac{1}{2}}\right) + \\ & \frac{k}{2}\left(\left(S_2^{(1)}\right)_{L+\frac{1}{2}}^{n+\frac{1}{2}} + \left(S_2^{(1)}\right)_{L-\frac{1}{2}}^{n+\frac{1}{2}}\right)\end{aligned} \tag{A.3}$$

and

$$(A^{(1)})_L^{n+1} = (A^{(1)})_L^n - \frac{k}{h}\left(\left(R_1^{(1)}\right)_{L+\frac{1}{2}}^{n+\frac{1}{2}} - \left(R_1^{(1)}\right)_{L-\frac{1}{2}}^{n+\frac{1}{2}}\right) \tag{A.4}$$

As in the case of the right boundary condition in section 1.3.2, we need a ghost point in order to determine $(\mathbf{R}^{(1)})_{L+\frac{1}{2}}^{n+\frac{1}{2}}$ and $(\mathbf{S}^{(1)})_{L+\frac{1}{2}}^{n+\frac{1}{2}}$,and hence $(Q^{(1)})_{L+\frac{1}{2}}^{n+\frac{1}{2}}$ and $(A^{(1)})_{L+\frac{1}{2}}^{n+\frac{1}{2}}$. The equations determinating the ghost point are given by

$$(Q^{(1)})_L^{n+\frac{1}{2}} = \frac{(Q^{(1)})_{L-\frac{1}{2}}^{n+\frac{1}{2}} + (Q^{(1)})_{L+\frac{1}{2}}^{n+\frac{1}{2}}}{2} \tag{A.5}$$

and

$$(A^{(1)})_L^{n+\frac{1}{2}} = \frac{(A^{(1)})_{L-\frac{1}{2}}^{n+\frac{1}{2}} + (A^{(1)})_{L+\frac{1}{2}}^{n+\frac{1}{2}}}{2} \tag{A.6}$$

The corresponding equations concerning the points on the left boundary of the second part of the tube (2) are given by

$$\begin{aligned}(Q^{(2)})_L^{n+1} = (Q^{(2)})_L^n &- \frac{k}{h}\left(\left(R_2^{(2)}\right)_{L+\frac{1}{2}}^{n+\frac{1}{2}} - \left(R_2^{(2)}\right)_{L-\frac{1}{2}}^{n+\frac{1}{2}}\right) + \\ &\frac{k}{2}\left(\left(S_2^{(2)}\right)_{L+\frac{1}{2}}^{n+\frac{1}{2}} + \left(S_2^{(2)}\right)_{L-\frac{1}{2}}^{n+\frac{1}{2}}\right)\end{aligned} \tag{A.7}$$

and

$$(A^{(2)})_L^{n+1} = (A^{(2)})_L^n - \frac{k}{h}\left(\left(R_1^{(2)}\right)_{L+\frac{1}{2}}^{n+\frac{1}{2}} - \left(R_1^{(2)}\right)_{L-\frac{1}{2}}^{n+\frac{1}{2}}\right) \tag{A.8}$$

Similar to the treatment of the left boundary, we need the ghost point to determine $(Q^{(2)})_{L-\frac{1}{2}}^{n+\frac{1}{2}}$ and $(A^{(2)})_{L-\frac{1}{2}}^{n+\frac{1}{2}}$. They are found from the approximations

$$(Q^{(2)})_L^{n+\frac{1}{2}} = \frac{(Q^{(2)})_{L-\frac{1}{2}}^{n+\frac{1}{2}} + (Q^{(2)})_{L+\frac{1}{2}}^{n+\frac{1}{2}}}{2} \tag{A.9}$$

and

$$(A^{(2)})_L^{n+\frac{1}{2}} = \frac{(A^{(2)})_{L-\frac{1}{2}}^{n+\frac{1}{2}} + (A^{(2)})_{L+\frac{1}{2}}^{n+\frac{1}{2}}}{2} \tag{A.10}$$

We now have twelve unknowns: $(Q^{(1)})_L^{n+1}$, $(Q^{(1)})_L^{n+\frac{1}{2}}$, $(Q^{(1)})_{L+\frac{1}{2}}^{n+\frac{1}{2}}$, $(A^{(1)})_L^{n+1}$, $(A^{(1)})_L^{n+\frac{1}{2}}$, $(A^{(1)})_{L+\frac{1}{2}}^{n+\frac{1}{2}}$, $(Q^{(2)})_L^{n+1}$, $(Q^{(2)})_L^{n+\frac{1}{2}}$, $(Q^{(2)})_{L-\frac{1}{2}}^{n+\frac{1}{2}}$, $(A^{(2)})_L^{n+1}$, $(A^{(2)})_L^{n+\frac{1}{2}}$, and $(A^{(2)})_{L-\frac{1}{2}}^{n+\frac{1}{2}}$. However, we have only eight equations. As in section 1.3.2 we apply the boundary

condition twice, namely at the time levels $(n+\frac{1}{2})$ and $(n+1)$. This adds the following two equations to the system.

$$(Q^{(1)})_L^{n+\frac{1}{2}} - (Q^{(2)})_L^{n+\frac{1}{2}} = \frac{(p^{(3)})_L - p_e}{(R^{(3)})_L^{n+\frac{1}{2}}} = \left(\frac{p_c^{(3)} \left(1 - \sqrt{\frac{A_0^{(3)}}{A^{(3)}}} \right) - p_e + p_0}{R^3} \right)_L^{n+\frac{1}{2}} \tag{A.11}$$

and

$$(Q^{(1)})_L^{n+1} - (Q^{(2)})_L^{n+1} = \frac{(p^{(3)})_L - p_e}{(R^{(3)})_L^{n+1}} = \left(\frac{p_c^{(3)} \left(1 - \sqrt{\frac{A_0^{(3)}}{A^{(3)}}} \right) - p_e + p_0}{R^{(3)}} \right)_L^{n+1} \tag{A.12}$$

In addition, we apply the relation (A.2) to obtain the too remaining equations

$$\begin{aligned} (p_c^{(1)})_L \left(1 - \sqrt{\frac{(A_0^{(1)})_L}{(A^{(1)})_L^{n+\frac{1}{2}}}} \right) &= (p_c^{(2)})_L \left(1 - \sqrt{\frac{(A_0^{(2)})_L}{(A^{(2)})_L^{n+\frac{1}{2}}}} \right) \\ &= (p_c^{(3)})_L \left(1 - \sqrt{\frac{(A_0^{(3)})_L}{(A^{(3)})_L^{n+\frac{1}{2}}}} \right) \end{aligned} \tag{A.13}$$

and

$$\begin{aligned} (p_c^{(1)})_L \left(1 - \sqrt{\frac{(A_0^{(1)})_L}{(A^{(1)})_L^{n+1}}} \right) &= (p_c^{(2)})_L \left(1 - \sqrt{\frac{(A_0^{(2)})_L}{(A^{(2)})_L^{n+1}}} \right) \\ &= (p_c^{(3)})_L \left(1 - \sqrt{\frac{(A_0^{(3)})_L}{(A^{(3)})_L^{n+1}}} \right) \end{aligned} \tag{A.14}$$

Using the above relations, it is possible to eliminate the right hand sides of (A.11) and (A.12). We have chosen to replace the right hand side by the expressions dealing with the first part of the tube[1].

If we let

$$\begin{aligned} x_1 &= (Q^{(1)})_L^{n+1} & x_2 &= (Q^{(1)})_L^{n+\frac{1}{2}} & x_3 &= (Q^{(1)})_{L+\frac{1}{2}}^{n+\frac{1}{2}} \\ x_4 &= (Q^{(2)})_L^{n+1} & x_5 &= (Q^{(2)})_L^{n+\frac{1}{2}} & x_6 &= (Q^{(2)})_{L-\frac{1}{2}}^{n+\frac{1}{2}} \\ x_7 &= (A^{(1)})_L^{n+1} & x_8 &= (A^{(1)})_L^{n+\frac{1}{2}} & x_9 &= (A^{(1)})_{L+\frac{1}{2}}^{n+\frac{1}{2}} \\ x_{10} &= (A^{(2)})_L^{n+1} & x_{11} &= (A^{(2)})_L^{n+\frac{1}{2}} & x_{12} &= (A^{(2)})_{L-\frac{1}{2}}^{n+\frac{1}{2}} \end{aligned}$$

[1] In both or in one of the cases one could just as well have replaced the right hand side by the expressions dealing with the second part of the tube.

and define $\theta = \frac{k}{h}$, and $\gamma = \frac{k}{2}$ we can use the above definitions to solve the equations (A.3-A.14), and thereby write the residuals in a more compact way. Further, we use the definitions of **R** and **S** (from page 14).

Equation 1 – from (A.3):

$$\begin{aligned} f_1 &= -x_1 + (Q^{(1)})_L^n - \theta \left(\frac{x_3^2}{x_9} + \frac{(p_c^{(1)})_{L+\frac{1}{2}} \sqrt{x_9 \, (A_0^{(1)})_{L+\frac{1}{2}}}}{\mathcal{F}^2} - \left(R_2^{(1)}\right)_{L-\frac{1}{2}}^{n+\frac{1}{2}} \right) + \\ & \gamma \left(F + \frac{x_9 (p_c^{(1)})_{L+\frac{1}{2}}}{(r^{(1)})_{L+\frac{1}{2}} \mathcal{F}^2} \left(\frac{dr^{(1)}}{dx} \right)_{L+\frac{1}{2}} + \frac{1}{\mathcal{F}^2} \left(2\sqrt{\pi x_9} - \frac{x_9}{(r^{(1)})_{L+\frac{1}{2}}^{n+\frac{1}{2}} \mathcal{F}^2} \right) \right. \\ & \left. \left(\frac{dEW}{dx} \right)_{L+\frac{1}{2}} + \left(S_2^{(1)}\right)_{L-\frac{1}{2}} \right) \end{aligned}$$

Let

$$\begin{aligned} k_1 &= \left(\frac{p_c^{(1)} \sqrt{A_0^{(1)}}}{\mathcal{F}^2} \right)_{L+\frac{1}{2}} \\ k_2 &= -8k\pi \frac{1}{\mathcal{R}} \\ k_3 &= \frac{2\sqrt{\pi}}{\mathcal{F}^2} \left(\frac{dEW}{dx} \right)_{L+\frac{1}{2}} \\ k_4 &= \left(\frac{p_c^{(1)}}{r^{(1)} \mathcal{F}^2} \frac{dr^{(1)}}{dx} - \frac{1}{r^{(1)} \mathcal{F}^2} \frac{dEW}{dx} \right)_{L+\frac{1}{2}} \end{aligned}$$

Using the definition (1.13) for FA, f_1 can be rewritten as

$$\begin{aligned} f_1 &= -x_1 + (Q^{(1)})_L^n - \theta \left(\frac{x_3^2}{x_9} + k_1 \sqrt{x_9} - \left(R_2^{(1)}\right)_{L-\frac{1}{2}}^{n+\frac{1}{2}} \right) + \\ & \gamma \left(k_2 \frac{x_3}{x_9} + k_3 \sqrt{x_9} + k_4 x_9 + \left(S_2^{(1)}\right)_{L-\frac{1}{2}}^{n+\frac{1}{2}} \right) \end{aligned}$$

Finally, if we let

$$g_1 = (Q^{(1)})_L^n + \theta \left(R_2^{(1)}\right)_{L-\frac{1}{2}}^{n+\frac{1}{2}} + \gamma \left(S_2^{(1)}\right)_{L-\frac{1}{2}}^{n+\frac{1}{2}}$$

then

$$f_1 = g_1 - x_1 - \theta \left(\frac{x_3^2}{x_9} + k_1 \sqrt{x_9} \right) + \gamma \left(k_2 \frac{x_3}{x_9} + k_3 \sqrt{x_9} + k_4 x_9 \right)$$

Equation 2 – from (A.4):

$$f_2 = -x_7 + (A^{(1)})_L^n - \theta\left(x_3 - \left(R_1^{(1)}\right)_{L-\frac{1}{2}}^{n+\frac{1}{2}}\right)$$

Let

$$k_5 = (A^{(1)})_L^n + \theta\left(R_1^{(1)}\right)_{L-\frac{1}{2}}^{n+\frac{1}{2}}$$

then

$$f_2 = -x_7 - \theta x_3 + k_5$$

Equation 3 – from (A.5):

$$f_3 = -x_2 + \frac{(Q^{(1)})_{L-\frac{1}{2}}^{n+\frac{1}{2}} + x_3}{2}$$

Let now

$$k_6 = \left(\frac{(Q^{(1)})}{2}\right)_{L-\frac{1}{2}}^{n+\frac{1}{2}}$$

then

$$f_3 = -x_2 + \frac{x_3}{2} + k_6$$

Equation 4 – from (A.6):

$$f_4 = -x_8 + \frac{(A^{(1)})_{L-\frac{1}{2}}^{n+\frac{1}{2}} + x_9}{2}$$

Let

$$k_7 = \left(\frac{(A^{(1)}}{2}\right)_{L-\frac{1}{2}}^{n+\frac{1}{2}}$$

then

$$f_4 = -x_8 + \frac{x_9}{2} + k_7$$

Equation 5 – from (A.7):

$$f_5 = -x_4 + (Q^{(2)})_L^n - \theta\left(\left(R_2^{(2)}\right)_{L+\frac{1}{2}}^{n+\frac{1}{2}} - \left(\frac{x_6^2}{x_{12}} + \frac{(p_c^{(2)})_{L-\frac{1}{2}}\sqrt{x_{12}\,(A_0^{(2)})_{L-\frac{1}{2}}}}{\mathcal{F}^2}\right)\right) +$$
$$\gamma\left(\left(S_2^{(2)}\right)_{L+\frac{1}{2}}^{n+\frac{1}{2}} + F + \frac{x_{12}(p_c^{(2)})_{L-\frac{1}{2}}}{(r^{(2)})_{L-\frac{1}{2}}^{n+\frac{1}{2}}\mathcal{F}^2}\left(\frac{dr^{(2)}}{dx}\right)_{L-\frac{1}{2}}^{n+\frac{1}{2}} + \right.$$
$$\left.\frac{1}{\mathcal{F}^2}\frac{1}{\mathcal{F}}^2\left(2\sqrt{\pi x_{12}} - \frac{x_{12}}{(r^{(2)})_{L-\frac{1}{2}}^{n+\frac{1}{2}}}\right)\left(\frac{dEW}{dx}\right)_{L-\frac{1}{2}}^{n+\frac{1}{2}}\right)$$

Let

$$k_8 = \left(\frac{p_c^{(2)}\sqrt{A_0^{(2)}}}{\mathcal{F}^2}\right)_{L-\frac{1}{2}}$$
$$k_9 = \frac{2\sqrt{\pi}}{\mathcal{F}^2}\left(\frac{dEW}{dx}\right)_{L-\frac{1}{2}}$$
$$k_{10} = \left(\frac{p_c^{(2)}}{r^{(2)}\mathcal{F}^2}\frac{dr^{(2)}}{dx} - \frac{1}{r^{(2)}\mathcal{F}^2}\frac{dEW}{dx}\right)_{L-\frac{1}{2}}$$

Using k_2 and the above, f_5 can be written as

$$f_5 = -x_4 + (Q^{(2)})_L^n - \theta\left(\left(R_2^{(2)}\right)_{L+\frac{1}{2}}^{n+\frac{1}{2}} - \left(\frac{x_6^2}{x_{12}} + k_8\sqrt{x_{12}}\right)\right) +$$
$$\gamma\left(\left(S_2^{(2)}\right)_{L+\frac{1}{2}}^{n+\frac{1}{2}} + k_2\frac{x_6}{x_{12}} + k_9\sqrt{x_{12}} + k_{10}x_{12}\right)$$

Finally, we let

$$g_2 = (Q^{(2)})_L^n - \theta\left(R_2^{(2)}\right)_{L+\frac{1}{2}}^{n+\frac{1}{2}} + \gamma\left(S_2^{(2)}\right)_{L+\frac{1}{2}}^{n+\frac{1}{2}}$$

then

$$f_5 = g_2 - x_4 + \theta\left(\frac{x_6^2}{x_{12}} + k_8\sqrt{x_{12}}\right) + \gamma\left(k_2\frac{x_6}{x_{12}} + k_9\sqrt{x_{12}} + k_{10}x_{12}\right)$$

Equation 6 – from (A.8):

$$f_6 = -x_{10} + (A^{(2)})_L^n - \theta\left(\left(R_1^{(2)}\right)_{L+\frac{1}{2}}^{n+\frac{1}{2}} - x_6\right)$$

Let

$$k_{11} = (A^{(2)})_L^n - \theta \left(R_1^{(2)}\right)_{L+\frac{1}{2}}^{n+\frac{1}{2}}$$

Then we can rewrite f_6 as

$$f_6 = -x_{10} + \theta x_6 + k_{11}$$

Equation 7 – from (A.9):

$$f_7 = -x_5 + \frac{x_6 + (Q^{(2)})_{L+\frac{1}{2}}^{n+\frac{1}{2}}}{2}$$

Let

$$k_{12} = \left(\frac{Q^{(2)}}{2}\right)_{L+\frac{1}{2}}^{n+\frac{1}{2}}$$

Then

$$f_7 = -x_5 + \frac{x_6}{2} + k_{12}$$

Equation 8 – from (A.10):

$$f_8 = -x_{11} + \frac{x_{12} + (A^{(2)})_{L+\frac{1}{2}}^{n+\frac{1}{2}}}{2}$$

Let

$$k_{13} = \left(\frac{A^{(2)}}{2}\right)_{L+\frac{1}{2}}^{n+\frac{1}{2}}$$

Then we get

$$f_8 = -x_{11} + \frac{x_{12}}{2} + k_{13}$$

Equation 9 – from (A.11):

$$f_9 = -x_2 + x_5 + \frac{(p_c^{(1)})_L^{n+\frac{1}{2}} \left(1 - \sqrt{\frac{(A_0^{(1)})_L}{x_8}}\right) + -p_e + p_0}{(R^{(3)})_L^{n+\frac{1}{2}}}$$

Let

$$k_{14} = \left(\frac{(p_c^{(1)}) - p_e + p_0}{R^{(3)}}\right)_L$$

$$k_{15} = \left(\frac{p_c^{(1)}\sqrt{A_0^{(1)}}}{R^{(3)}}\right)_L$$

Then f_9 can be simplified as

$$f_9 = -x_2 + x_5 + k_{14} - \frac{k_{15}}{\sqrt{x_8}}$$

Equation 10 – from (A.12):

$$f_{10} = -x_1 + x_4 + \frac{(p_c^{(1)})_L\left(1 - \sqrt{\frac{(A_0^{(1)})_L}{x_7}}\right) - p_e + p_0}{R^{(3)}}$$

The constants k_{14} and k_{15} are reused since p_c and A_0 are not dependent of time. Therefore

$$f_{10} = -x_1 + x_4 + k_{14} - \frac{k_{15}}{\sqrt{x_7}}$$

Equation 11 – from (A.13):

$$f_{11} = -(p_c^{(1)})_L\left(1 - \sqrt{\frac{(A_0^{(1)})_L}{x_8}}\right) + (p_c^{(2)})_L\left(1 - \sqrt{\frac{(A_0^{(2)})_L}{x_{11}}}\right)$$

Let

$$k_{16} = -\left(p_c^{(1)} + p_c^{(2)}\right)_L$$

$$k_{17} = \left(p_c^{(1)}\sqrt{A_0^{(1)}}\right)_L$$

$$k_{18} = \left(p_c^{(2)}\sqrt{A_0^{(2)}}\right)_L$$

Then f_{11} can be written as

$$f_{11} = \frac{k_{17}}{\sqrt{x_8}} - \frac{k_{18}}{\sqrt{x_{11}}} + k_{16}$$

Equation 12 – from (A.14):

$$f_{12} = -(p_c^{(1)})_L \left(1 - \sqrt{\frac{(A_0^{(1)})_L}{x_7}}\right) + (p_c^{(2)})_L \left(1 - \sqrt{\frac{(A_0^{(2)})_L}{x_{10}}}\right)$$

Since neither p_c nor A_0 depends on t, we can reuse the constants $k_{16} - k_{18}$. Doing so, f_{12} can be rewritten as

$$f_{12} = \frac{k_{17}}{\sqrt{x_7}} - \frac{k_{18}}{\sqrt{x_{10}}} + k_{16}$$

In order to solve these twelve equations using Newton's method (see page 21 and [4], [19]) we need to specify the Jacobian of the system. Having this matrix, we can follow the same recipe as for the right boundary condition in section 1.3.2.

The Jacobian is given by:

$$D\mathbf{f} = \begin{pmatrix}
-1 & 0 & \xi_1 & 0 & 0 & 0 & 0 & 0 & \xi_2 & 0 & 0 & 0 \\
0 & 0 & -\theta & 0 & 0 & 0 & -1 & 0 & 0 & 0 & 0 & 0 \\
0 & -1 & \frac{1}{2} & 0 & 0 & 0 & 0 & 0 & 0 & 0 & 0 & 0 \\
0 & 0 & 0 & 0 & 0 & 0 & 0 & -1 & \frac{1}{2} & 0 & 0 & 0 \\
0 & 0 & 0 & -1 & 0 & \xi_3 & 0 & 0 & 0 & 0 & 0 & \xi_4 \\
0 & 0 & 0 & 0 & 0 & \theta & 0 & 0 & 0 & -1 & 0 & 0 \\
0 & 0 & 0 & 0 & -1 & \frac{1}{2} & 0 & 0 & 0 & 0 & 0 & 0 \\
0 & 0 & 0 & 0 & 0 & 0 & 0 & 0 & 0 & 0 & -1 & \frac{1}{2} \\
0 & -1 & 0 & 0 & 1 & 0 & 0 & \frac{k_{15}}{2x_8^{3/2}} & 0 & 0 & 0 & 0 \\
-1 & 0 & 0 & 1 & 0 & 0 & \frac{k_{15}}{2x_7^{3/2}} & 0 & 0 & 0 & 0 & 0 \\
0 & 0 & 0 & 0 & 0 & 0 & 0 & -\frac{k_{17}}{2x_8^{3/2}} & 0 & 0 & \frac{k_{18}}{2x_{11}^{3/2}} & 0 \\
0 & 0 & 0 & 0 & 0 & 0 & -\frac{k_{17}}{2x_7^{3/2}} & 0 & 0 & \frac{k_{18}}{2x_{10}^{3/2}} & 0 & 0
\end{pmatrix}$$

where

$$\begin{aligned}
\xi_1 &= \frac{-2\theta x_3 + \gamma k_2}{x_9} \\
\xi_2 &= -\theta\left(-\frac{x_3^2}{x_9^2} + \frac{k_1}{2\sqrt{x_9}}\right) + \gamma\left(-k_2\frac{x_3}{x_9^2} + \frac{k_3}{2\sqrt{x_9}} + k_4\right) \\
\xi_3 &= \frac{2\theta x_6 + \gamma k_2}{x_{12}} \\
\xi_4 &= \theta\left(-\frac{x_6^2}{x_{12}^2} + \frac{k_8}{2\sqrt{x_{12}}}\right) + \gamma\left(-k_2\frac{x_6}{x_{12}^2} + \frac{k_9}{2\sqrt{x_{12}}} + k_{10}\right)
\end{aligned}$$

In the case of B in figure 5.2, we have that $A^{(1)}(L,t) = A^{(2)}(L,t)$ and the number of equations can be reduced, since the conditions in (A.13) and (A.14) are not necessary. Following this, it is easily seen that the unknowns $(A^{(1)})_L^{n+1}$ and $(A^{(1)})_L^{n+\frac{1}{2}}$ coincide with the corresponding unknowns for $A^{(2)}$. Further, the unknowns $(A^{(1)})_{L+\frac{1}{2}}^{n+\frac{1}{2}}$ and $(A^{(2)})_{L-\frac{1}{2}}^{n+\frac{1}{2}}$ are already known from the tubes 2 and 1, respectively. Therefore, neither of the equations (A.6) and (A.10) are necessary. The result of this simplification is that we in the case of B in figure 5.2 are left with eight equations having eight unknowns.

Appendix B

A discrete outflow using a separate segment containing the branch

In this section we will develop the equations necessary for treating a bifurcation point of type A in figure 5.2. First of all, assume that the mass is conserved, hence

$$Q^{(1)} - Q^{(2)} - \frac{d}{dt}\int_L^{L+\xi} A\,dx = Q^{(3)} = \frac{p^{(3)}}{R^{(3)}} \tag{B.1}$$

where

$$\frac{d}{dt}\int_L^{L+\xi} A\,dx = \frac{d}{dt}\left(A^{(1)} + A^{(2)} + \sqrt{A^{(1)}A^{(2)}}\right)$$

if we as shown in figure 5.2.A assume that the tube taper linearly in the bifurcation segment. Secondly we apply Bernoulli's relation.

$$\begin{aligned} p^{(1)} &= p^{(2)} + \frac{\rho}{2}\left((v^{(2)})^2 + (v^{(1)})^2\right) + \rho\int_L^{L+\xi}\frac{\partial v}{\partial t}\,ds + \Delta p^{(2)} \\ &= p^{(3)} + \frac{\rho}{2}\left((v^{(3)})^2 + (v^{(1)})^2\right) + \rho\int_L^{L+\frac{\xi}{2}}\frac{\partial v}{\partial t}\,ds + \Delta p^{(3)} \end{aligned}$$

where $\Delta p^{(i)}$, $i = 2, 3$ is accounting for the friction loss due to the curvature of the branches being considered. The integral is discretized using a backward discretization scheme. Thus

$$\rho\int_{x_1}^{x_2}\frac{\partial v}{\partial t}\,ds = \frac{\rho\xi}{2\Delta t}\left(v(x_1,t) + v(x_2,t) - (v(x_1,t-\Delta t) + v(x_2,t-\Delta t)\right)$$

These assumptions are presented by Stettler[25] and Skalak[22]. Similarly, a backward discretization of the time-derivative in (B.1) is used. If the time level $t = n + 1$ and $t - \Delta t = n$ we get

$$\frac{d}{dt}\frac{\xi}{3}\left((A^{(1)})^{n+1} + (A^{(2)})^{n+1} + \sqrt{(A^{(1)})^{n+1}(A^{(2)})^{n+1}}\right) =$$
$$\frac{\xi}{3}\frac{(A^{(1)})^{n+1} + (A^{(2)})^{n+1} + \sqrt{(A^{(1)}A^{(2)})^{n+1}} - \left((A^{(1)})^{n} + (A^{(2)})^{n} + \sqrt{(A^{(1)}A^{(2)})^{n}}\right)}{\Delta t}$$

Using the fact that $v = \frac{Q}{A}$, the definition of $p(A)$, and the latter condition we get the requirements

$$\left(p_c^{(1)}\left(1 - \sqrt{\frac{A_0^{(1)}}{A^{(1)}}}\right)\right)_L^{n+1}$$
$$= \left(p_c^{(2)}\left(1 - \sqrt{\frac{A_0^{(2)}}{A^{(2)}}}\right)\right)_{L+\xi}^{n+1} + \frac{\rho}{2}\left(\left(\left(\frac{Q^{(2)}}{A^{(2)}}\right)^2\right)_{L+\xi}^{n+1} + \left(\left(\frac{Q^{(1)}}{A^{(1)}}\right)^2\right)_{L}^{n+1}\right) + \tag{B.2}$$
$$\frac{\rho\xi}{k}\left(\left(\frac{Q^{(1)}}{A^{(1)}}\right)_L^{n+1} + \left(\frac{Q^{(2)}}{A^{(2)}}\right)_{L+\xi}^{n+1} - \left(\left(\frac{Q^{(1)}}{A^{(1)}}\right)_L^{n+\frac{1}{2}} + \left(\frac{Q^{(2)}}{A^{(2)}}\right)_{L+\xi}^{n+\frac{1}{2}}\right)\right) + \left(\Delta p^{(2)}\right)_{L+\xi}$$
$$= \left(p_c^{(3)}\left(1 - \sqrt{\frac{A_0^{(3)}}{A^{(3)}}}\right)\right)_{L+\frac{\xi}{2}}^{n+1} + \frac{\rho}{2}\left(\left(\left(\frac{Q^{(3)}}{A^{(3)}}\right)^2\right)_{L+\frac{\xi}{2}}^{n+1} + \left(\left(\frac{Q^{(1)}}{A^{(1)}}\right)^2\right)_{L}^{n+1}\right) + \tag{B.3}$$
$$\frac{\rho\xi}{k}\left(\left(\frac{Q^{(1)}}{A^{(1)}}\right)_L^{n+1} + \left(\frac{Q^{(3)}}{A^{(3)}}\right)_{L+\frac{\xi}{2}}^{n+1} - \left(\left(\frac{Q^{(1)}}{A^{(1)}}\right)_L^{n+\frac{1}{2}} + \left(\frac{Q^{(3)}}{A^{(3)}}\right)_{L+\frac{\xi}{2}}^{n+\frac{1}{2}}\right)\right) + \left(\Delta p^{(3)}\right)_{L+\frac{\xi}{2}}$$

Seen from the first part of the tube (1), the equations at the points on the right boundary are

$$(Q^{(1)})_L^{n+1} = (Q^{(1)})_L^n - \frac{k}{h}\left(\left(R_2^{(1)}\right)_{L+\frac{1}{2}}^{n+\frac{1}{2}} - \left(R_2^{(1)}\right)_{L-\frac{1}{2}}^{n+\frac{1}{2}}\right) + \frac{k}{2}\left(\left(S_2^{(1)}\right)_{L+\frac{1}{2}}^{n+\frac{1}{2}} + \left(S_2^{(1)}\right)_{L-\frac{1}{2}}^{n+\frac{1}{2}}\right) \tag{B.4}$$

and

$$(A^{(1)})_L^{n+1} = (A^{(1)})_L^n - \frac{k}{h}\left(\left(R_1^{(1)}\right)_{L+\frac{1}{2}}^{n+\frac{1}{2}} - \left(R_1^{(1)}\right)_{L-\frac{1}{2}}^{n+\frac{1}{2}}\right) \tag{B.5}$$

As in the case of the right boundary condition in section 1.3.2, we need a ghost point in order to determine $(\mathbf{R}^{(1)})_{L+\frac{1}{2}}^{n+\frac{1}{2}}$ and $(\mathbf{S}^{(1)})_{L+\frac{1}{2}}^{n+\frac{1}{2}}$ – and hence $(Q^{(1)})_{L+\frac{1}{2}}^{n+\frac{1}{2}}$ and $(A^{(1)})_{L+\frac{1}{2}}^{n+\frac{1}{2}}$. The equations determinating the ghost point are given by

$$(Q^{(1)})_L^{n+\frac{1}{2}} = \frac{(Q^{(1)})_{L-\frac{1}{2}}^{n+\frac{1}{2}} + (Q^{(1)})_{L+\frac{1}{2}}^{n+\frac{1}{2}}}{2} \tag{B.6}$$

and

$$(A^{(1)})_L^{n+\frac{1}{2}} = \frac{(A^{(1)})_{L-\frac{1}{2}}^{n+\frac{1}{2}} + (A^{(1)})_{L+\frac{1}{2}}^{n+\frac{1}{2}}}{2} \tag{B.7}$$

The corresponding equations concerning the points on the left boundary of the second part of the tube are given by

$$\begin{aligned}(Q^{(2)})_{L+\xi}^{n+1} &= (Q^{(2)})_{L+\xi}^{n} - \frac{k}{h}\left(\left(R_2^{(2)}\right)_{L+\xi+\frac{1}{2}}^{n+\frac{1}{2}} - \left(R_2^{(2)}\right)_{L+\xi-\frac{1}{2}}^{n+\frac{1}{2}}\right) + \\ &\quad \frac{k}{2}\left(\left(S_2^{(2)}\right)_{L+\xi+\frac{1}{2}}^{n+\frac{1}{2}} + \left(S_2^{(2)}\right)_{L+\xi-\frac{1}{2}}^{n+\frac{1}{2}}\right)\end{aligned} \tag{B.8}$$

and

$$(A^{(2)})_{L+\xi}^{n+1} = (A^{(2)})_{L+\xi}^{n} - \frac{k}{h}\left(\left(R_1^{(2)}\right)_{L+\xi+\frac{1}{2}}^{n+\frac{1}{2}} - \left(R_1^{(2)}\right)_{L+\xi-\frac{1}{2}}^{n+\frac{1}{2}}\right) \tag{B.9}$$

Similar to the treatment of the left boundary, we need the ghost point to determine $(Q^{(2)})_{L+\xi-\frac{1}{2}}^{n+\frac{1}{2}}$ and $(A^{(2)})_{L+\xi-\frac{1}{2}}^{n+\frac{1}{2}}$. They are found from the approximations

$$(Q^{(2)})_{L+\xi}^{n+\frac{1}{2}} = \frac{(Q^{(2)})_{L+\xi-\frac{1}{2}}^{n+\frac{1}{2}} + (Q^{(2)})_{L+\xi+\frac{1}{2}}^{n+\frac{1}{2}}}{2} \tag{B.10}$$

and

$$(A^{(2)})_{L+\xi}^{n+\frac{1}{2}} = \frac{(A^{(2)})_{L+\xi-\frac{1}{2}}^{n+\frac{1}{2}} + (A^{(2)})_{L+\xi+\frac{1}{2}}^{n+\frac{1}{2}}}{2} \tag{B.11}$$

We now have twelve unknowns: $(Q^{(1)})_L^{n+1}$, $(Q^{(1)})_L^{n+\frac{1}{2}}$, $(Q^{(1)})_{L+\frac{1}{2}}^{n+\frac{1}{2}}$, $(A^{(1)})_L^{n+1}$, $(A^{(1)})_L^{n+\frac{1}{2}}$, $(A^{(1)})_{L+\frac{1}{2}}^{n+\frac{1}{2}}$, $(Q^{(2)})_{L+\xi}^{n+1}$, $(Q^{(2)})_{L+\xi}^{n+\frac{1}{2}}$, $(Q^{(2)})_{L+\xi-\frac{1}{2}}^{n+\frac{1}{2}}$, $(A^{(2)})_{L+\xi}^{n+1}$, $(A^{(2)})_{L+\xi}^{n+\frac{1}{2}}$, and $(A^{(2)})_{L+\xi-\frac{1}{2}}^{n+\frac{1}{2}}$. However, we have only eight equations. As in section 1.3.2 we apply the boundary condition twice, namely at the time levels $(n+\frac{1}{2})$ and $(n+1)$. This adds the following two equations to the system.

$$\begin{aligned}&(Q^{(1)})_L^{n+\frac{1}{2}} - (Q^{(2)})_{L+\xi}^{n+\frac{1}{2}} - \\ &\frac{2\xi}{3k}\left((A^{(1)})_L^{n+\frac{1}{2}} + (A^{(2)})_{L+\xi}^{n+\frac{1}{2}} + \sqrt{(A^{(1)})_L^{n+\frac{1}{2}}(A^{(2)})_{L+\xi}^{n+\frac{1}{2}}} - \right. \\ &\left.\left((A^{(1)})_L^{n} + (A^{(2)})_{L+\xi}^{n} + \sqrt{(A^{(1)})_L^{n}(A^{(2)})_{L+\xi}^{n}}\right)\right) = \\ &\frac{(p^{(3)})_{L+\frac{\xi}{2}}^{n+\frac{1}{2}}}{R^{(3)}} = \left(\frac{p_c^{(3)}\left(1-\sqrt{\frac{A_0^{(3)}}{A^{(3)}}}\right) - p_e + p_0}{R^{(3)}}\right)_{L+\frac{\xi}{2}}^{n+\frac{1}{2}}\end{aligned} \tag{B.12}$$

and

$$
\begin{aligned}
&(Q^{(1)})_L^{n+1} - (Q^{(2)})_{L+\xi}^{n+1} - \\
&\frac{2\xi}{3k}\left((A^{(1)})_L^{n+1} + (A^{(2)})_{L+\xi}^{n+1} + \sqrt{(A^{(1)})_L^{n+1}(A^{(2)})_{L+\xi}^{n+1}} - \right. \\
&\left.\left((A^{(1)})_L^{n+\frac{1}{2}} + (A^{(2)})_{L+\xi}^{n+\frac{1}{2}} + \sqrt{(A^{(1)})_L^{n+\frac{1}{2}}(A^{(2)})_{L+\xi}^{n+\frac{1}{2}}}\right)\right) = \\
&\frac{(p^{(3)})_{L+\frac{\xi}{2}}^{n+1}}{R^{(3)}} = \left(\frac{p_c^{(3)}\left(1 - \sqrt{\frac{A_0^{(3)}}{A^{(3)}}}\right) - p_e + p_0}{R^{(3)}}\right)_{L+\frac{\xi}{2}}^{n+1}
\end{aligned}
\tag{B.13}
$$

Introducing the boundary conditions adds two more unknowns to the system namely $(A^{(3)})_{L+\frac{\xi}{2}}^{n+\frac{1}{2}}$ and $(A^{(3)})_{L+\frac{\xi}{2}}^{n+1}$. However, if we apply the relation (B.4) we are able to obtain the remaining equations

$$
\begin{aligned}
&(p_c^{(1)})_L\left(1 - \sqrt{\frac{(A_0^{(1)})_L}{(A^{(1)})_L^{n+\frac{1}{2}}}}\right) \\
&= (p_c^{(2)})_{L+\xi}\left(1 - \sqrt{\frac{(A_0^{(2)})_{L+\xi}}{(A^{(2)})_{L+\xi}^{n+\frac{1}{2}}}}\right) + \frac{\rho}{2}\left(\left(\frac{(Q^{(2)})_{L+\xi}^{n+\frac{1}{2}}}{(A^{(2)})_{L+\xi}^{n+\frac{1}{2}}}\right)^2 + \left(\frac{(Q^{(1)})_L^{n+\frac{1}{2}}}{(A^{(1)})_L^{n+\frac{1}{2}}}\right)^2\right) + \\
&\frac{\rho\xi}{2k}\left(\frac{(Q^{(1)})_L^{n+\frac{1}{2}}}{(A^{(1)})_L^{n+\frac{1}{2}}} + \frac{(Q^{(2)})_{L+\xi}^{n+\frac{1}{2}}}{(A^{(2)})_{L+\xi}^{n+\frac{1}{2}}} - \left(\frac{(Q^{(1)})_L^{n}}{(A^{(1)})_L^{n}} + \frac{(Q^{(2)})_{L+\xi}^{n}}{(A^{(2)})_{L+\xi}^{n}}\right)\right) + \\
&\left(\Delta p^{(2)}\right)_{L+\xi}
\end{aligned}
\tag{B.14}
$$

$$
\begin{aligned}
&= (p_c^{(3)})_{L+\frac{\xi}{2}}\left(1 - \sqrt{\frac{(A_0^{(3)})_{L+\frac{\xi}{2}}}{(A^{(3)})_{L+\frac{\xi}{2}}^{n+\frac{1}{2}}}}\right) + \frac{\rho}{2}\left(\left(\frac{(Q^{(3)})_{L+\frac{\xi}{2}}^{n+\frac{1}{2}}}{(A^{(3)})_{L+\frac{\xi}{2}}^{n+\frac{1}{2}}}\right)^2 + \left(\frac{(Q^{(1)})_L^{n+\frac{1}{2}}}{(A^{(1)})_L^{n+\frac{1}{2}}}\right)^2\right) + \\
&\frac{\rho\xi}{k}\left(\frac{(Q^{(1)})_L^{n+\frac{1}{2}}}{(A^{(1)})_L^{n+\frac{1}{2}}} + \frac{(Q^{(3)})_{L+\frac{\xi}{2}}^{n+\frac{1}{2}}}{(A^{(3)})_{L+\frac{\xi}{2}}^{n+\frac{1}{2}}} - \left(\frac{(Q^{(1)})_L^{n}}{(A^{(1)})_L^{n}} + \frac{(Q^{(3)})_{L+\frac{\xi}{2}}^{n}}{(A^{(3)})_{L+\frac{\xi}{2}}^{n}}\right)\right) + \\
&\left(\Delta p^{(3)}\right)_{L+\frac{\xi}{2}}
\end{aligned}
\tag{B.15}
$$

Using the relation at time level $n+1$ yields:

$$
(p_c^{(1)})_L\left(1 - \sqrt{\frac{(A_0^{(1)})_L}{(A^{(1)})_L^{n+1}}}\right)
$$

$$= (p_c^{(2)})_{L+\xi}\left(1-\sqrt{\frac{(A_0^{(2)})_{L+\xi}}{(A^{(2)})_{L+\xi}^{n+1}}}\right)+\frac{\rho}{2}\left(\left(\frac{(Q^{(2)})_{L+\xi}^{n+1}}{(A^{(2)})_{L+\xi}^{n+1}}\right)^2+\left(\frac{(Q^{(1)})_L^{n+1}}{(A^{(1)})_L^{n+1}}\right)^2\right) \quad \text{(B.16)}$$

$$+\frac{\rho\xi}{2}\left(\frac{(Q^{(1)})_L^{n+1}}{(A^{(1)})_L^{n+1}}+\frac{(Q^{(2)})_{L+\xi}^{n+1}}{(A^{(2)})_{L+\xi}^{n+1}}-\left(\frac{(Q^{(1)})_L^{n+\frac{1}{2}}}{(A^{(1)})_L^{n+\frac{1}{2}}}+\frac{(Q^{(2)})_{L+\xi}^{n+\frac{1}{2}}}{(A^{(2)})_{L+\xi}^{n+\frac{1}{2}}}\right)\right)+\left(\Delta p^{(2)}\right)_{L+\xi}$$

$$= (p_c^{(3)})_{L+\frac{\xi}{2}}\left(1-\sqrt{\frac{(A_0^{(3)})_{L+\frac{\xi}{2}}}{(A^{(3)})_{L+\frac{\xi}{2}}^{n+1}}}\right)+\frac{\rho}{2}\left(\left(\frac{(Q^{(3)})_{L+\frac{\xi}{2}}^{n+1}}{(A^{(3)})_{L+\frac{\xi}{2}}^{n+1}}\right)^2+\left(\frac{(Q^{(1)})_L^{n+1}}{(A^{(1)})_L^{n+1}}\right)^2\right) \quad \text{(B.17)}$$

$$+\frac{\rho\xi}{k}\left(\frac{(Q^{(1)})_L^{n+1}}{(A^{(1)})_L^{n+1}}+\frac{(Q^{(3)})_{L+\frac{\xi}{2}}^{n+1}}{(A^{(3)})_{L+\frac{\xi}{2}}^{n+1}}-\left(\frac{(Q^{(1)})_L^{n+\frac{1}{2}}}{(A^{(1)})_L^{n+\frac{1}{2}}}+\frac{(Q^{(3)})_{L+\frac{\xi}{2}}^{n+\frac{1}{2}}}{(A^{(3)})_{L+\frac{\xi}{2}}^{n+\frac{1}{2}}}\right)\right)+\left(\Delta p^{(3)}\right)_{L+\frac{\xi}{2}}$$

If we let

$$\begin{array}{lll}
x_1=(Q^{(1)})_L^{n+1} & x_2=(Q^{(1)})_L^{n+\frac{1}{2}} & x_3=(Q^{(1)})_{L+\frac{1}{2}}^{n+\frac{1}{2}} \\
x_4=(Q^{(2)})_{L+\xi}^{n+1} & x_5=(Q^{(2)})_{L+\xi}^{n+\frac{1}{2}} & x_6=(Q^{(2)})_{L+\xi-\frac{1}{2}}^{n+\frac{1}{2}} \\
x_7=(A^{(1)})_L^{n+1} & x_8=(A^{(1)})_L^{n+\frac{1}{2}} & x_9=(A^{(1)})_{L+\frac{1}{2}}^{n+\frac{1}{2}} \\
x_{10}=(A^{(2)})_{L+\xi}^{n+1} & x_{11}=(A^{(2)})_{L+\xi}^{n+\frac{1}{2}} & x_{12}=(A^{(2)})_{L+\xi-\frac{1}{2}}^{n+\frac{1}{2}} \\
x_{13}=(A^{(3)})_{L+\frac{\xi}{2}}^{n+\frac{1}{2}} & x_{14}=(A^{(3)})_{L+\frac{\xi}{2}}^{n+1} &
\end{array}$$

and define $\theta=\frac{k}{h}$, and $\gamma=\frac{k}{2}$ we can use the above definitions to solve the equations (B.4-B.17), and thereby write the residuals in a more compact way. Further, we use the definitions of **R** and **S** (from page 14).

Equation 1 – from (B.4):

$$f_1 = -x_1+(Q^{(1)})_L^n-\theta\left(\frac{x_3^2}{x_9}+\frac{(p_c^{(1)})_{L+\frac{1}{2}}\sqrt{x_9\,(A_0^{(1)})_{L+\frac{1}{2}}}}{\mathcal{F}^2}-\left(R_2^{(1)}\right)_{L-\frac{1}{2}}^{n+\frac{1}{2}}\right)+$$

$$\gamma\left(F+\frac{x_9(p_c^{(1)})_{L+\frac{1}{2}}}{(r^{(1)})_{L+\frac{1}{2}}\mathcal{F}^2}\left(\frac{dr^{(1)}}{dx}\right)_{L+\frac{1}{2}}+\frac{1}{\mathcal{F}^2}\left(2\sqrt{\pi x_9}-\frac{x_9}{(r^{(1)})_{L+\frac{1}{2}}}\right)\right.$$

$$\left.\left(\frac{dEW}{dx}\right)_{L+\frac{1}{2}}+\left(S_2^{(1)}\right)_{L-\frac{1}{2}}^{n+\frac{1}{2}}\right)$$

Let

$$k_1 = \left(\frac{p_c^{(1)}\sqrt{A_0^{(1)}}}{\mathcal{F}^2}\right)_{L+\frac{1}{2}}$$

$$
\begin{aligned}
k_2 &= -8k\pi\frac{1}{\mathcal{R}} \\
k_3 &= \frac{2\sqrt{\pi}}{\mathcal{F}^2}\left(\frac{dEW}{dx}\right)_{L+\frac{1}{2}} \\
k_4 &= \left(\frac{p_c^{(1)}}{r^{(1)}\mathcal{F}^2}\frac{dr^{(1)}}{dx} - \frac{1}{r^{(1)}\mathcal{F}^2}\frac{dEW}{dx}\right)_{L+\frac{1}{2}}
\end{aligned}
$$

Using the definition (1.13) for FA, f_1 can be rewritten as

$$
\begin{aligned}
f_1 &= -x_1 + (Q^{(1)})_L^n - \theta\left(\frac{x_3^2}{x_9} + k_1\sqrt{x_9} - \left(R_2^{(1)}\right)_{L-\frac{1}{2}}^{n+\frac{1}{2}}\right) + \\
&\quad \gamma\left(k_2\frac{x_3}{x_9} + k_3\sqrt{x_9} + k_4 x_9 + \left(S_2^{(1)}\right)_{L-\frac{1}{2}}^{n+\frac{1}{2}}\right)
\end{aligned}
$$

Finally, if we let

$$
g_1 = (Q^{(1)})_L^n + \theta\left(R_2^{(1)}\right)_{L-\frac{1}{2}}^{n+\frac{1}{2}} + \gamma\left(S_2^{(1)}\right)_{L-\frac{1}{2}}^{n+\frac{1}{2}}
$$

then

$$
f_1 = g_1 - x_1 - \theta\left(\frac{x_3^2}{x_9} + k_1\sqrt{x_9}\right) + \gamma\left(k_2\frac{x_3}{x_9} + k_3\sqrt{x_9} + k_4 x_9\right)
$$

Equation 2 – from (B.5):

$$
f_2 = -x_7 + (A^{(1)})_L^n - \theta\left(x_3 - \left(R_1^{(1)}\right)_{L-\frac{1}{2}}^{n+\frac{1}{2}}\right)
$$

Let

$$
k_5 = (A^{(1)})_L^n + \theta\left(R_1^{(1)}\right)_{L-\frac{1}{2}}^{n+\frac{1}{2}}
$$

then

$$
f_2 = -x_7 - \theta x_3 + k_5
$$

Equation 3 – from (B.6):

$$
f_3 = -x_2 + \frac{(Q^{(1)})_{L-\frac{1}{2}}^{n+\frac{1}{2}} + x_3}{2}
$$

Let now

$$k_6 = \left(\frac{Q^{(1)}}{2}\right)^{n+\frac{1}{2}}_{L-\frac{1}{2}}$$

then

$$f_3 = -x_2 + \frac{x_3}{2} + k_6$$

Equation 4 – from (B.7):

$$f_4 = -x_8 + \frac{(A^{(1)})^{n+\frac{1}{2}}_{L-\frac{1}{2}} + x_9}{2}$$

Let

$$k_7 = \left(\frac{A^{(1)}}{2}\right)^{n+\frac{1}{2}}_{L-\frac{1}{2}}$$

then

$$f_4 = -x_8 + \frac{x_9}{2} + k_7$$

Equation 5 – from (B.8):

$$\begin{aligned} f_5 = & -x_4 + (Q^{(2)})^n_{L+\xi} \\ & -\theta\left(\left(R_2^{(2)}\right)^{n+\frac{1}{2}}_{L+\xi+\frac{1}{2}} - \left(\frac{x_6^2}{x_{12}} + \frac{(p_c^{(2)})_{L+\xi-\frac{1}{2}}\sqrt{x_{12}\,(A_0^{(2)})_{L+\xi-\frac{1}{2}}}}{\mathcal{F}^2}\right)\right) + \\ & \gamma\left(\left(S_2^{(2)}\right)^{n+\frac{1}{2}}_{L+\xi+\frac{1}{2}} + F + \frac{x_{12}(p_c^{(2)})_{L+\xi-\frac{1}{2}}}{(r^{(2)})_{L+\xi-\frac{1}{2}}\mathcal{F}^2}\left(\frac{dr^{(2)}}{dx}\right)_{L+\xi-\frac{1}{2}} + \right. \\ & \left. \frac{1}{\mathcal{F}^2}\left(2\sqrt{\pi x_{12}} - \frac{x_{12}}{(r^{(2)})_{L+\xi-\frac{1}{2}}}\right)\left(\frac{dEW}{dx}\right)_{L-\frac{1}{2}}\right) \end{aligned}$$

Let

$$k_8 = \left(\frac{p_c^{(2)}\sqrt{A_0^{(2)}}}{\mathcal{F}^2}\right)_{L+\xi-\frac{1}{2}}$$

$$k_9 = \frac{2\sqrt{\pi}}{\mathcal{F}^2}\left(\frac{dEW}{dx}\right)_{L-\frac{1}{2}}$$

$$k_{10} = \left(\frac{p_c^{(2)}}{r^{(2)}\mathcal{F}^2}\frac{dr^{(2)}}{dx} - \frac{1}{r^{(2)}\mathcal{F}^2}\frac{dEW}{dx}\right)_{L+\xi-\frac{1}{2}}$$

Using k_2 and the above, f_5 can be written as

$$f_5 = -x_4 + (Q^{(2)})^n_{L+\xi} - \theta\left(\left(R_2^{(2)}\right)^{n+\frac{1}{2}}_{L+\xi+\frac{1}{2}} - \left(\frac{x_6^2}{x_{12}} + k_8\sqrt{x_{12}}\right)\right) + \gamma\left(\left(S_2^{(2)}\right)^{n+\frac{1}{2}}_{L+\xi+\frac{1}{2}} + k_2\frac{x_6}{x_{12}} + k_9\sqrt{x_{12}} + k_{10}x_{12}\right)$$

Finally, we let

$$g_2 = (Q^{(2)})^n_{L+\xi} - \theta\left(R_2^{(2)}\right)^{n+\frac{1}{2}}_{L+\xi+\frac{1}{2}} + \gamma\left(S_2^{(2)}\right)^{n+\frac{1}{2}}_{L+\xi+\frac{1}{2}}$$

then

$$f_5 = g_2 - x_4 + \theta\left(\frac{x_6^2}{x_{12}} + k_8\sqrt{x_{12}}\right) + \gamma\left(k_2\frac{x_6}{x_{12}} + k_9\sqrt{x_{12}} + k_{10}x_{12}\right)$$

Equation 6 – from (B.9):

$$f_6 = -x_{10} + (A^{(2)})^n_{L+\xi} - \theta\left(\left(R_1^2\right)^{n+\frac{1}{2}}_{L+\xi+\frac{1}{2}} - x_6\right)$$

Let

$$k_{11} = (A^{(2)})^n_{L+\xi} - \theta\left(R_1^2\right)^{n+\frac{1}{2}}_{L+\xi+\frac{1}{2}}$$

Then we can rewrite f_6 as

$$f_6 = -x_{10} + \theta x_6 + k_{11}$$

Equation 7 – from (B.10):

$$f_7 = -x_5 + \frac{x_6 + (Q^{(2)})^{n+\frac{1}{2}}_{L+\xi+\frac{1}{2}}}{2}$$

Let

$$k_{12} = \left(\frac{Q^{(2)}}{2}\right)^{n+\frac{1}{2}}_{L+\xi+\frac{1}{2}}$$

Then

$$f_7 = -x_5 + \frac{x_6}{2} + k_{12}$$

Equation 8 – from (B.11):

$$f_8 = -x_{11} + \frac{x_{12} + (A^{(2)})^{n+\frac{1}{2}}_{L+\xi+\frac{1}{2}}}{2}$$

Let

$$k_{13} = \left(\frac{A^{(2)}}{2}\right)^{n+\frac{1}{2}}_{L+\xi+\frac{1}{2}}$$

Then we get

$$f_8 = -x_{11} + \frac{x_{12}}{2} + k_{13}$$

Equation 9 – from (B.12):

$$\begin{aligned} f_9 = & -x_2 + x_5 + \\ & \frac{2\xi}{3k}\left(x_8 + x_{11} + \sqrt{x_8 x_{11}} - \left((A^{(1)})^n_L + (A^{(2)})^n_{L+\xi} + \sqrt{(A^{(1)})^n_L (A_2)^n_{L+\xi}}\right)\right) + \\ & \frac{(p_c^{(3)})_L\left(1 - \sqrt{\frac{(A_0^{(3)})_L}{x_{13}}}\right) - p_e + p_0}{R^{(3)}} \end{aligned}$$

Let

$$\begin{aligned} k_{14} &= \frac{2\xi}{3k} \\ k_{15} &= -\frac{2\xi}{3k}\left((A_1)^n_L + (A_2)^n_{L+\xi} + \sqrt{(A_1)^n_L (A_2)^n_{L+\xi}}\right) + \frac{(p_c^{(3)})_{L+\frac{\xi}{2}} - p_e + p_0}{R^{(3)}} \\ k_{16} &= -\frac{(p_c^{(3)})^{n+\frac{1}{2}}_{L+\frac{\xi}{2}}\sqrt{(A_0^{(3)})_L}}{R^{(3)}} \end{aligned}$$

Then f_9 can be simplified as

$$f_9 = -x_2 + x_5 + k_{14}\left(x_8 + x_{11} + \sqrt{x_8 x_{11}}\right) + k_{15} + \frac{k_{16}}{\sqrt{x_{13}}}$$

Equation 10 – from (B.13):

$$f_{10} = -x_1 + x_4 + \frac{2\xi}{3k}\left(x_7 + x_{10} + \sqrt{x_7 x_{10}} - \left(x_8 + x_{11} + \sqrt{x_8 x_{11}}\right)\right) + \frac{\left(p_c^{(3)}\right)_{L+\frac{\xi}{2}}\left(1 - \sqrt{\frac{\left(A_0^{(3)}\right)_L}{x_{13}}}\right) - p_e + p_0}{R^{(3)}}$$

The constants k_{14} and k_{16} are reused since p_c and A_0 are not dependent of time. If we then let

$$k_{17} = \frac{\left(p_c^{(3)}\right)_{L+\frac{\xi}{2}} - p_e + p_0}{R^{(3)}}$$

Then

$$f_{10} = -x_1 + x_4 + k_{14}\left(x_7 + x_{10} + \sqrt{x_7 x_{10}} - \left(x_8 + x_{11} + \sqrt{x_8 x_{11}}\right)\right) + k_{17} + \frac{k_{16}}{\sqrt{x_{14}}}$$

Equation 11 – from (B.14):

$$f_{11} = -\left(p_c^{(1)}\right)_L\left(1 - \sqrt{\frac{\left(A_0^{(1)}\right)_L}{x_8}}\right) + \left(p_c^2\right)_{L+\xi}\left(1 - \sqrt{\frac{\left(A_0^{(2)}\right)_{L+\xi}}{x_{11}}}\right) + \frac{\rho}{2}\left(\left(\frac{x_5}{x_{11}}\right)^2 + \left(\frac{x_2}{x_8}\right)^2\right) + \frac{\rho\xi}{k}\left(\frac{x_5}{x_{11}} + \frac{x_2}{x_8} - \left(\frac{\left(Q^{(1)}\right)_L^n}{\left(A^{(1)}\right)_L^n} + \frac{\left(Q^{(2)}\right)_{L+\xi}^n}{\left(A_2\right)_{L+\xi}^n}\right)\right) + \left(\Delta p^{(2)}\right)_{L+\xi}$$

Let

$$k_{18} = -\left(p_c^{(1)}\right)_L + \left(p_c^{(2)}\right)_{L+\xi} - \frac{\rho\xi}{k}\left(\frac{\left(Q^{(1)}\right)_L^n}{\left(A_1\right)_L^n} + \frac{\left(Q^{(2)}\right)_{L+\xi}^n}{\left(A^{(2)}\right)_{L+\xi}^n}\right) + \left(\Delta p^{(2)}\right)_{L+\xi}$$

$$k_{19} = \left(p_c^{(1)}\sqrt{\left(A_0^{(1)}\right)}\right)_L$$

$$k_{20} = -\left(p_c^{(2)}\sqrt{\left(A_0^{(2)}\right)}\right)_{L+\xi}$$

$$k_{21} = \frac{\rho}{2}$$

$$k_{22} = \frac{\rho\xi}{k}$$

Then f_{11} can be written as

$$f_{11} = \frac{k_{19}}{\sqrt{x_8}} + \frac{k_{20}}{\sqrt{x_{11}}} + k_{18} + k_{21}\left(\left(\frac{x_5}{x_{11}}\right)^2 + \left(\frac{x_2}{x_8}\right)^2\right) + k_{22}\left(\frac{x_5}{x_{11}} + \frac{x_2}{x_8}\right)$$

Equation 12 – from (B.15):

$$f_{12} = -(p_c^{(1)})_L\left(1 - \sqrt{\frac{(A_0^{(1)})_L}{x_8}}\right) + (p_c^{(3)})_{L+\frac{\xi}{2}}\left(1 - \sqrt{\frac{(A_0^{(3)})_{L+\frac{\xi}{2}}}{x_{13}}}\right) + \frac{\rho}{2}\left(\left(\frac{(Q_3)^{n+\frac{1}{2}}_{L+\frac{\xi}{2}}}{x_{13}}\right)^2 + \left(\frac{x_2}{x_8}\right)^2\right) + \frac{\rho\xi}{k}\left(\frac{(Q_3)^{n+\frac{1}{2}}_{L+\frac{\xi}{2}}}{x_{13}} + \frac{x_2}{x_8} - \left(\frac{(Q^{(1)})^n_L}{(A^{(1)})^n_L} + \frac{(Q^{(3)})^n_{L+\frac{\xi}{2}}}{(A_3)^n_{L+\frac{\xi}{2}}}\right)\right) + \left(\Delta p^{(3)}\right)_{L+\frac{\xi}{2}}$$

Reusing the constants k_{19}, k_{21}, k_{22}, and letting

$$k_{23} = -(p_c^{(1)})_L + (p_c^{(3)})_{L+\frac{\xi}{2}} - \frac{\rho\xi}{k}\left(\frac{(Q^{(1)})^n_L}{(A_1)^n_L} + \frac{(Q^{(3)})^n_{L+\frac{\xi}{2}}}{(A^{(3)})^n_{L+\frac{\xi}{2}}}\right) + \left(\Delta p^{(3)}\right)_{L+\frac{\xi}{2}}$$

$$k_{24} = -\left(p_c^{(3)}\sqrt{(A_0^{(3)}}\right)_{L+\frac{\xi}{2}}$$

where

$$(Q^{(3)})^{n+\frac{1}{2}}_{L+\frac{\xi}{2}} = \frac{(p^{(3)})_{L+\frac{\xi}{2}}}{R^{(3)}} = \frac{(p_c^{(3)})_{L+\frac{\xi}{2}}\left(1 - \sqrt{\frac{(A_0^{(3)})_{L+\frac{\xi}{2}}}{x_{13}}}\right) - p_e + p_0}{R^{(3)}} = k_{25} + \frac{k_{26}}{\sqrt{x_{13}}}$$

If

$$k_{25} = \frac{(p_c^{(3)})_{L+\frac{\xi}{2}} - p_e + p_0}{R^{(3)}}$$

$$k_{26} = -\frac{(p_c^{(3)})_{L+\frac{\xi}{2}}\sqrt{(A_0^{(3)})_{L+\frac{\xi}{2}}}}{R^{(3)}}$$

Then f_{12} can be written as

$$f_{12} = \frac{k_{19}}{\sqrt{x_8}} + \frac{k_{24}}{\sqrt{x_{13}}} + k_{23} + k_{21}\left(\left(\frac{k_{25} + \frac{k_{26}}{\sqrt{x_{13}}}}{x_{13}}\right)^2 + \left(\frac{x_2}{x_8}\right)^2\right) + k_{22}\left(\frac{k_{25} + \frac{k_{26}}{\sqrt{x_{13}}}}{x_{13}} + \frac{x_2}{x_8}\right)$$

Equation 13 – from (B.16):

$$f_{13} = -(p_c^{(1)})_L\left(1 - \sqrt{\frac{(A_0^{(1)})_L}{x_7}}\right) + (p_c^{(2)})_{L+\xi}\left(1 - \sqrt{\frac{(A_0^{(2)})_{L+\xi}}{x_{10}}}\right) + \frac{\rho}{2}\left(\left(\frac{x_4}{x_{10}}\right)^2 + \left(\frac{x_1}{x_7}\right)^2\right) + \frac{\rho\xi}{k}\left(\frac{x_4}{x_{10}} + \frac{x_1}{x_7} - \left(\frac{x_2}{x_8} + \frac{x_5}{x_{11}}\right)\right)$$

Since neither p_c nor A_0 depends on t, we can reuse the constants k_{19}, k_{20}, k_{22}, and k_{23}. Letting

$$k_{27} = -(p_c^{(1)})_L + (p_c^{(2)})_{L+\xi} + (\Delta p^{(2)})_{L+\xi}$$

Doing so, f_{13} can be rewritten as

$$f_{13} = \frac{k_{19}}{\sqrt{x_7}} + \frac{k_{20}}{\sqrt{x_{10}}} + k_{23} + k_{27}\left(\left(\frac{x_4}{x_{10}}\right)^2 + \left(\frac{x_1}{x_7}\right)^2\right) + k_{22}\left(\frac{x_4}{x_{10}} + \frac{x_1}{x_7} - \left(\frac{x_2}{x_8} + \frac{x_5}{x_{11}}\right)\right)$$

Equation 14 – from (B.17):

$$f_{14} = -(p_c^{(1)})_L\left(1 - \sqrt{\frac{(A_0^{(1)})_L}{x_7}}\right) + (p_c^{(3)})_{L+\frac{\xi}{2}}\left(1 - \sqrt{\frac{(A_0^{(3)})_{L+\frac{\xi}{2}}}{x_{14}}}\right) + \frac{\rho}{2}\left(\left(\frac{(Q_3)_{L+\frac{\xi}{2}}^{n+1}}{x_{14}}\right)^2 + \left(\frac{x_1}{x_7}\right)^2\right) + \frac{\rho\xi}{k}\left(\frac{(Q_3)_{L+\frac{\xi}{2}}^{n+1}}{x_{14}} + \frac{x_1}{x_7} - \left(\frac{x_2}{x_8} + \frac{(Q^{(3)})_{L+\frac{\xi}{2}}^{n+\frac{1}{2}}}{x_{13}}\right)\right) + \left(\Delta p^{(3)}\right)_{L+\frac{\xi}{2}}$$

It is possible to use some of the constants defined previously. Let

$$k_{28} = -(p_c^{(1)})_L + (p_c^{(3)})_{L+\frac{\xi}{2}} + \left(\Delta p^{(3)}\right)_{L+\frac{\xi}{2}}$$

and

$$
\begin{aligned}
(Q^{(3)})^{n+1}_{L+\frac{\xi}{2}} &= \frac{(p^{(3)})_{L+\frac{\xi}{2}}}{R^{(3)}} \\
&= \frac{(p_c^{(3)})_{L+\frac{\xi}{2}} \left(1 - \sqrt{\frac{(A_0^{(3)})_{L+\frac{\xi}{2}}}{x_{14}}}\right) - p_e + p_0}{R^{(3)}} = k_{25} + \frac{k_{26}}{\sqrt{x_{14}}}
\end{aligned}
$$

where we have reused k_25 and k_{26} since p_c and A_0 do not depend on t.

Using the definition of $(Q^{(3)})^{n+\frac{1}{2}}_{L+\frac{\xi}{2}}$ from equation 12 and the above, we get the following expression for f_{14}

$$
\begin{aligned}
f_{14} = \frac{k_{19}}{\sqrt{x_7}} + \frac{k_{24}}{\sqrt{x_{14}}} + k_{28} + k_{21}\left(\left(\frac{k_{25} + \frac{k_{26}}{\sqrt{x_{14}}}}{x_{14}}\right)^2 + \left(\frac{x_1}{x_7}\right)^2\right) + \\
k_{22}\left(\frac{k_{25} + \frac{k_{26}}{\sqrt{x_{14}}}}{x_{14}} + \frac{x_1}{x_7} - \left(\frac{x_2}{x_8} + \frac{k_{25} + \frac{k_{26}}{\sqrt{x_{13}}}}{x_{13}}\right)\right)
\end{aligned}
$$

In order to solve these fourteen equations using Newton's method (see page 21 and [4], [19]) we need to specify the Jacobian of the system. Having this matrix, we can follow the same recipe as for the right boundary condition in section 1.3.2.

The Jacobian $D\mathbf{f}$ is given by:

$$
\begin{pmatrix}
-1 & 0 & \xi_1 & 0 & 0 & 0 & 0 & 0 & \xi_2 & 0 & 0 & 0 & 0 & 0 \\
0 & 0 & -\theta & 0 & 0 & 0 & -1 & 0 & 0 & 0 & 0 & 0 & 0 & 0 \\
0 & -1 & \frac{1}{2} & 0 & 0 & 0 & 0 & 0 & 0 & 0 & 0 & 0 & 0 & 0 \\
0 & 0 & 0 & 0 & 0 & 0 & 0 & -1 & \frac{1}{2} & 0 & 0 & 0 & 0 & 0 \\
0 & 0 & 0 & -1 & 0 & \xi_3 & 0 & 0 & 0 & 0 & 0 & \xi_4 & 0 & 0 \\
0 & 0 & 0 & 0 & 0 & \theta & 0 & 0 & 0 & -1 & 0 & 0 & 0 & 0 \\
0 & 0 & 0 & 0 & -1 & \frac{1}{2} & 0 & 0 & 0 & 0 & 0 & 0 & 0 & 0 \\
0 & 0 & 0 & 0 & 0 & 0 & 0 & 0 & 0 & 0 & -1 & \frac{1}{2} & 0 & 0 \\
0 & -1 & 0 & 0 & 1 & 0 & 0 & \xi_5 & 0 & 0 & \xi_6 & 0 & \frac{k_{16}}{2x_{13}^{3/2}} & 0 \\
-1 & 0 & 0 & 1 & 0 & 0 & \xi_7 & \xi_8 & 0 & \xi_9 & \xi_{10} & 0 & 0 & -\frac{k_{16}}{2x_{14}^{3/2}} \\
0 & \xi_{11} & 0 & 0 & \xi_{12} & 0 & 0 & \xi_{13} & 0 & 0 & \xi_{14} & 0 & 0 & 0 \\
0 & \xi_{15} & 0 & 0 & 0 & 0 & 0 & \xi_{16} & 0 & 0 & 0 & 0 & \xi_{17} & 0 \\
\xi_{18} & -\frac{k_{22}}{x_8} & 0 & \xi_{19} & -\frac{k_{22}}{x_{11}} & 0 & \xi_{20} & \frac{k_{22}x_2}{x_8^2} & 0 & \xi_{21} & -\frac{k_{22}x_5}{x_{11}^2} & 0 & 0 & 0 \\
\xi_{22} & -\frac{k_{22}}{x_8} & 0 & 0 & 0 & 0 & \xi_{23} & \frac{k_{22}x_2}{x_8^2} & 0 & 0 & 0 & 0 & \xi_{24} & \xi_{25}
\end{pmatrix}
$$

where

$$
\begin{aligned}
\xi_1 &= \frac{-2\theta x_3 + \gamma k_2}{x_9} \\
\xi_2 &= -\theta\left(-\frac{x_3^2}{x_9^2} + \frac{k_1}{2\sqrt{x_9}}\right) + \gamma\left(-k_2\frac{x_3}{x_9^2} + \frac{k_3}{2\sqrt{x_9}} + k_4\right) \\
\xi_3 &= \frac{2\theta x_6 + \gamma k_2}{x_{12}} \\
\xi_4 &= \theta\left(-\frac{x_6^2}{x_{12}^2} + \frac{k_8}{2\sqrt{x_{12}}}\right) + \gamma\left(-k_2\frac{x_6}{x_{12}^2} + \frac{k_9}{2\sqrt{x_{12}}} + k_{10}\right) \\
\xi_5 &= k_{14}\left(1 + \frac{\sqrt{x_{11}}}{2\sqrt{x_8}}\right) \\
\xi_6 &= k_{14}\left(1 + \frac{\sqrt{x_8}}{2\sqrt{x_{11}}}\right) \\
\xi_7 &= k_{14}\left(1 + \frac{\sqrt{x_{10}}}{2\sqrt{x_7}}\right) \\
\xi_8 &= -1 - \frac{\sqrt{x_{11}}}{2\sqrt{x_8}} \\
\xi_9 &= k_{14}\left(1 + \frac{\sqrt{x_7}}{2\sqrt{x_{10}}}\right) \\
\xi_{10} &= -1 - \frac{\sqrt{x_8}}{2\sqrt{x_{11}}} \\
\xi_{11} &= 2k_{21}\frac{x_2}{x_8^2} + \frac{k_{22}}{x_8} \\
\xi_{12} &= 2k_{21}\frac{x_5}{x_{11}^2} + \frac{k_{22}}{x_{11}} \\
\xi_{13} &= -\frac{k_{19}}{2x_8^{3/2}} - \frac{2k_{21}x_2^2}{x_8^3} - \frac{k_{22}x_2}{x_8^2} \\
\xi_{14} &= -\frac{k_{20}}{2x_{11}^{3/2}} - \frac{2k_{21}x_5^2}{x_{11}^3} - \frac{k_{22}x_5}{x_{11}^2} \\
\xi_{15} &= \frac{2k_{21}x_2}{x_8^2} + \frac{k_{22}}{x_8} \\
\xi_{16} &= -\frac{k_{19}}{2x_8^{3/2}} - \frac{2k_{21}x_2^2}{x_8^3} - \frac{k_{22}x_2}{x_8^2} \\
\xi_{17} &= -\frac{k_{24}}{2x_{13}^{3/2}} + \left(2k_{21}\left(k_{25} + \frac{k_{26}}{\sqrt{x_{13}}}\right) - k_{22}\right)\left(\frac{-x_{13}\frac{k_{26}}{2x_{13}^{3/2}} - \left(k_{25} + \frac{k_{26}}{\sqrt{x_{13}}}\right)}{x_{13}^2}\right) \\
\xi_{18} &= 2\frac{k_{27}x_1}{x_7^2} + \frac{k_{22}}{x_7}
\end{aligned}
$$

$$\xi_{19} = 2\frac{k_{27}x_4}{x_{10}^2} + \frac{k_{22}}{x_{10}}$$

$$\xi_{20} = -\frac{-k_{19}}{2x_7^{3/2}} - \frac{2k_{27}x_1^2}{x_7^3} - \frac{k_{22}x_1}{x_7^2}$$

$$\xi_{21} = -\frac{k_{20}}{2x_{10}^{3/2}} - \frac{2k_{27}x_4^2}{x_{10}^3} - \frac{k_{22}x_4}{x_{10}^2}$$

$$\xi_{22} = 2\frac{k_{27}x_1}{x_7^2} + \frac{k_{22}}{x_7}$$

$$\xi_{23} = -\frac{k_{19}}{2x_7^{3/2}} - \frac{2k_{21}x_1^2}{x_7^3} - \frac{k_{22}x_1}{x_7^2}$$

$$\xi_{24} = k_{22}\frac{x_{13}\frac{k_{26}}{2x_{13}^{3/2}} - \left(k_{25} + \frac{k_{26}}{\sqrt{x_{13}}}\right)}{x_{13}^2}$$

$$\xi_{25} = -\frac{k_{24}}{2x_{14}^{3/2}} + \left(2k_{21}\left(k_{25} + \frac{k_{26}}{\sqrt{x_{14}}}\right) - k_{22}\right)\left(\frac{-x_{14}\frac{k_{26}}{2x_{14}^{3/2}} - \left(k_{25} + \frac{k_{26}}{\sqrt{x_{14}}}\right)}{x_{14}^2}\right)$$

Bibliography

[1] G. Alberi, Z. Bajzer, and P. Baxa, editors. *Baromodulation as the Cause of Short Term Blood Pressure Variability*. Proceedings of the International Conference on Applications of Physics to Medicine and Biology, World Scientific, 1982.

[2] M. Anliker, J.C. Stettler, P. Niederer, and R. Holenstein. Prediction of shape changes of propagating flow and pressure pulses in human arteries. In R.D. Bauer and R. Busse, editors, *Dynamics, Control Theory and Regulation*, pages 15–34. Symposium at Erlangen on 28-30 Oktober 1977, 1977.

[3] Max Anliker, Robert L Rockwell, and Eric Ogden. Nonlinear analysis of flow pulses and shock waves in arteries. *Zeitschrift für Angewendte Matematik und Physik*, 22:217–245, 1971.

[4] Bulirsch and Stoer. *Introduction to Numerical Analysis*. Springer Verlag, Texts in Applied Mathematics 12, second edition, 1992.

[5] Per Foege Jensen, Henning Boje Andersen, Finn R. Nielsen, and Stig Andur Pedersen. The anaesthesia simulator sophus. Technical Report Risø-R-718(EN), Risoe National Laboratory, Roskilde, Denmark, November 1991. **Note:** The report describes the concept and the use of the anaesthesia simulator Sophus.

[6] Sir James Lighthill. *Mathematical Biofluiddynamics*. Regional Conference Series in Applied Mathematics. Society for Industrial and Apllied mathematics, third printing edition, 1989.

[7] M. Lister. The numerical solution of hyperbolic partial differential equations by the method of characteristics. In A. Ralston and H.S. Wilf, editors, *Mathematical Methods for Digital Computers*. John Wiley & Sons, 1960.

[8] Jagan N. Mazumdar. *Biofluid Mechanics*. World Scientific, Singapore, 1992.

[9] Donald A. McDonald. *Blood Flow in Arteries*. Edward Arnold, second edition edition, 1974.

[10] Finn R. Nielsen, Per Føge Jensen, and Stig Andur Pedersen. Pawi - patient anaesthetic workstation interface. The sophus simulator developed by Herlev University Hospital, Risø National Laboratory and Roskilde University Centre., 1993.

[11] A. Noordergraaf. *Circulatory System Dynamics*. Academic Press, 1978.

[12] A. Noordergraaf, P.D. Verdouw, A.G.W. Van Brummelen, and F.W. Wiegel. *Analog of the Arterial Bed in Pulsatile Blood Flow*. McGraw-Hill Book Company, New York, 1964.

[13] Abraham Noordergraaf. *Hemodynamics in Biological Engineering*. McGraw-Hill Book Company, New York, 1969.

[14] Mette Olufsen, Finn Nielsen, Per Føge Jensen, and Stig Andur Pedersen. The models underlying the anaesthesia simulator sophus. Imfufatekst nr 278, Roskilde University, Denmark, 1994.

[15] J. Paquerot and S. Lambrakos. Monovariable representation of blood flow in a large elastic artery. *Phys. Rev. E*, 49:3432–3439, 1994.

[16] T.J. Pedley. *The Fluid Mechanics of Large Blood Vessels*. Cambridge University Press, 1980.

[17] Charles Peskin. *Partial Differential Equations in Biology*. Lecutre Notes from CIMS at New York University. The Courant Institute of Mathematical Sciences, New Yourk University, 1976.

[18] Charles Peskin and F.C. Hoppensteadt. *Mathematics in Medicine and the Life Sciences, in the Heart and Circulation*. Springer Verlag, 1992.

[19] William H. Press, Saul A. Teukolsky, William T. Vetterling, and Brian P. Flannery. *Numerical Recipes in C - The Art of Scientific Computing*. Cambridge University Press, second edition, 1992.

[20] P. Reuderink, H. Hoogstraten, P. Sipkema, B. Hillen, and N. Westerhof. Linear and nonlinear one-dimensional models of pulse wave transmission at high womersley numbers. *J. Biomech.*, 22:819–827, 1989.

[21] T. Nørgaard, J. Ellegaard, J. Jalving, J. B. Pedersen, P. Gregersen, S. I. Meyer, and Henrik Wittus. Aortamodellering. Projektrapport 4 semester Naturfaglig Basisudannelse - Roskilde Universitetscenter., 1993.

[22] R. Skalak and S. Chien. *Handbook of Bioengineering*. McGraw-Hill, 1986.

[23] Richard Skalak, Nihat Özkaya, and Thomas C. Skalak. Biofluid mechanics. *Annual Review of Fluid Mechanics*, 21:167–205, 1989.

[24] J. Stettler, P. Niederer, and M. Anliker. Theoretical analysis of arterial hemodynamics including the influence of bifurcations, part 1. *Ann. Biomed. Eng.*, 9:145–164, 1981.

[25] J.C. Stettler, P. Niederer, and M. Anliker. Theoretical analysis of arterial hemodynamics including the influence of bifurcations, part i: Mathematical model and prediction of normal pulse patterns. *Annals of Biomedical Engineering*, 9:145–164, 1981.

[26] K. Sunagawa and K. Sagawa. Models of ventricular contraction based on time-varying elastance. *CRC, Critical Reviews in Biomedical Engineering*, 1982.

[27] N. Westerhof, G. Elzinga, and P. Sikema. An artificial system for pumping hearts. *Journal of Applied Physiology*, 31, 1971.

[28] N. Westerhof and A. Noordergraaf. Wave travel and input impedance for various types of networks in an electrical model of the human systemic arterial tree, with and without elastic tapering. In *Proceedings of the 19'th Annual Conference on Engineering in Medicine and Biology*, San Francisco, 1966.

[29] L. Zheng and Y. Wen-Jei. A computer simulation of the non-newtonian blood flow at the aortic bifurcation. *J. Biomech.*, 26:37–49, 1993.